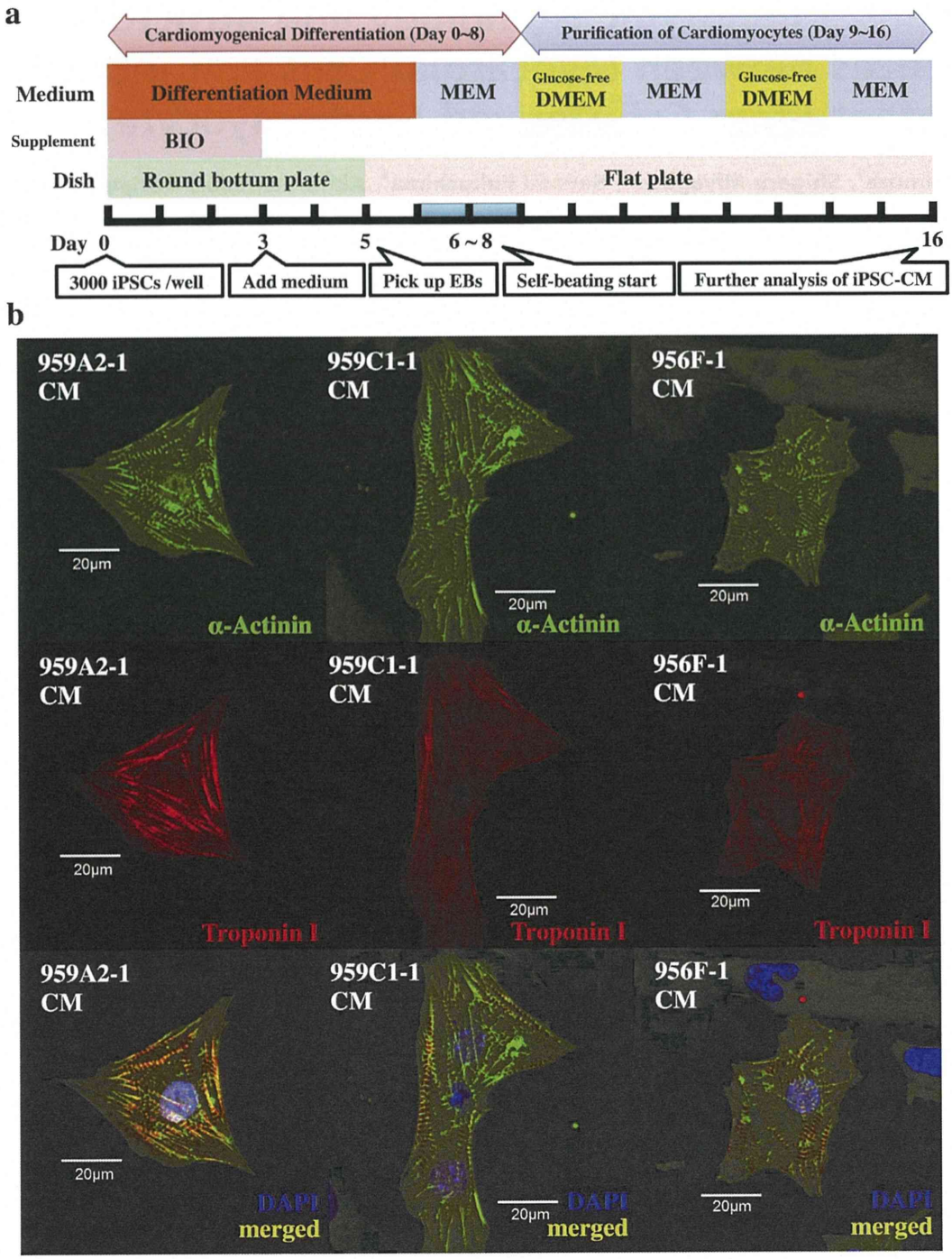

Figure 1. Cardiomyogenic differentiation of iPSCs and cardiomyocyte purification. (a) The cardiomyogenic differentiation protocol and cardiomyocyte purification process are illustrated. (b) IPSC-CMs stained with anti-α-actinin antibody (Alexa Fluor 488), anti-troponin I (Alexa Fluor 594) and DAPI, were analyzed with a confocal laser scanning microscopy. Abbreviations: EB, embryonic body; MEM, Modified Eagle's Medium; DMEM, Dulbecco's Modified Eagle's Medium; BIO, 6-bromoindirubin-3′-oxime.
doi:10.1371/journal.pone.0111064.g001

change during the course of cardiomyogenic differentiation of iPSCs *in vitro*. We analyzed *N*-glycan expression in undifferentiated iPSCs, iPSC-CMs, and adult murine myocardium by HPLC, to identify potential indicators of the maturity of differentiating cardiomyocytes from iPS cells *in vitro*.

Materials and Methods

Animal care procedures were consistent with the "Guide for the Care and Use of Laboratory Animals" (National Institutes of Health publication). Experimental protocols were approved by the

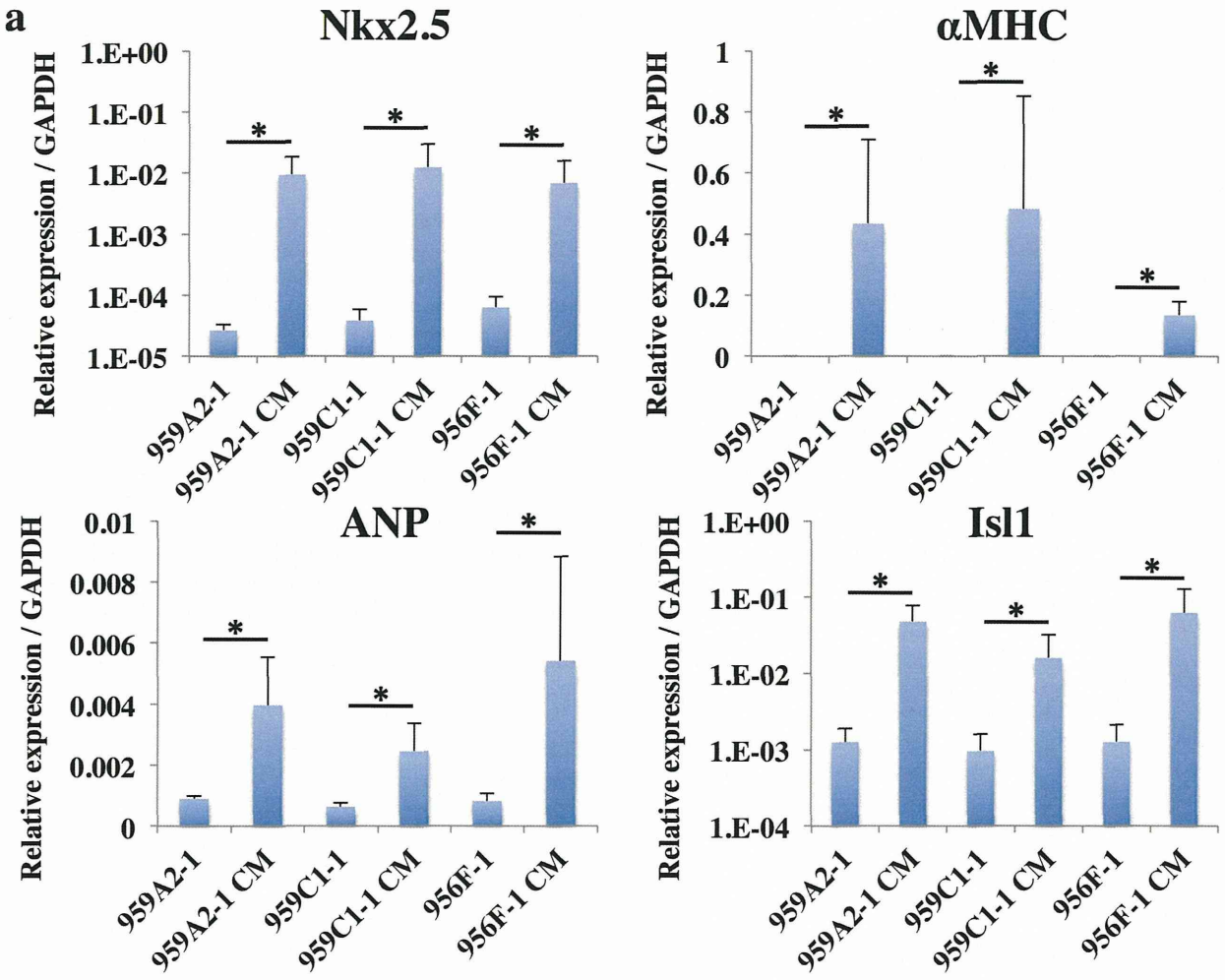
a
Nkx2.5
αMHC
ANP
Isl1
Relative expression / GAPDH
1.E+00
1.E-01
1.E-02
1.E-03
1.E-04
1.E-05
1
0.8
0.6
0.4
0.2
0
0.01
0.008
0.006
0.004
0.002
959A2-1
959A2-1 CM
959C1-1
959C1-1 CM
956F-1
956F-1 CM

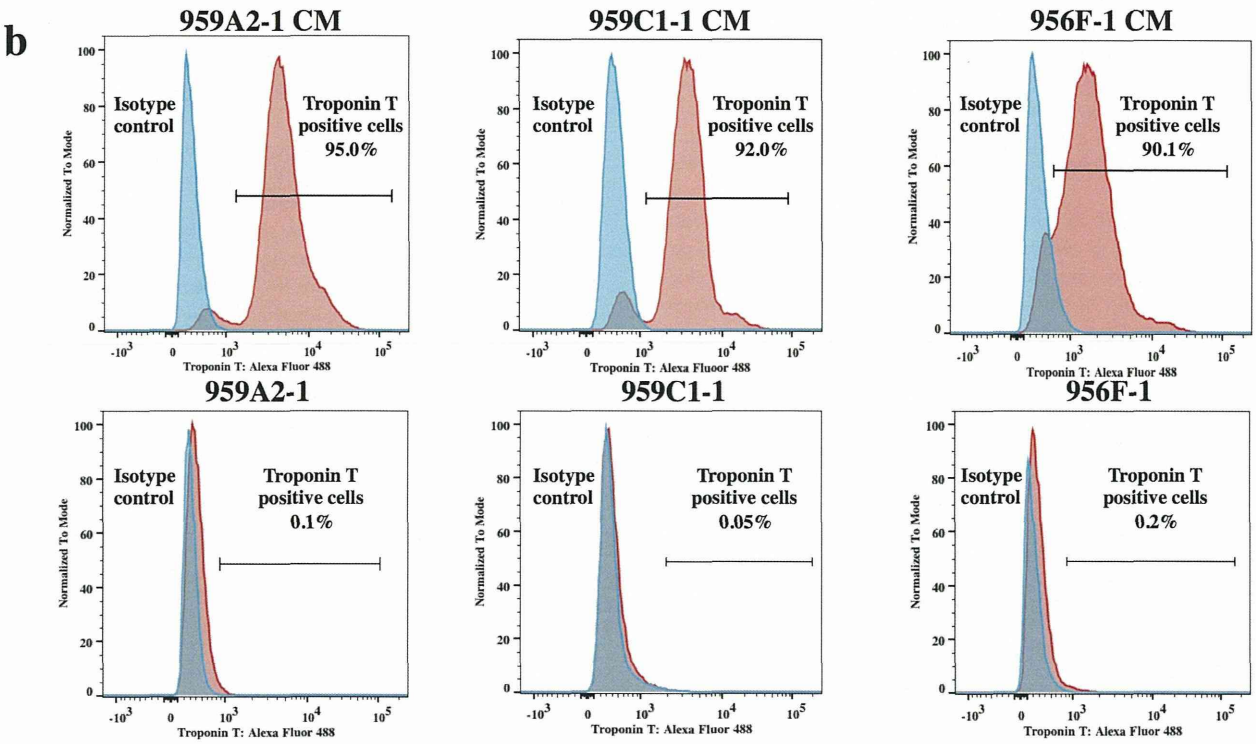
b
959A2-1 CM
959C1-1 CM
956F-1 CM
959A2-1
959C1-1
956F-1
Isotype control
Troponin T positive cells 95.0%
Troponin T positive cells 92.0%
Troponin T positive cells 90.1%
Troponin T positive cells 0.1%
Troponin T positive cells 0.05%
Troponin T positive cells 0.2%
Normalized To Mode
Troponin T: Alexa Fluor 488

Figure 2. Highly purified iPSC-CMs expressing cardiomyocyte marker genes. (a) Transcript expression of Nkx2.5, αMHC, ANP and Isl1 in the iPSCs and the iPSC-CMs were analyzed by real-time PCR. Results are expressed as the mean ± standard deviation. *P<0.05. (b) IPSC-CMs and iPSCs stained with anti-troponin T antibody or the isotype control, followed by Alexa Fluor 488-conjugated anti-mouse IgG antibody, were analyzed by flow cytometry.
doi:10.1371/journal.pone.0111064.g002

Ethics Review Committee for Animal Experimentation of Osaka University Graduate School of Medicine.

Cardiomyogenic differentiation of murine iPSCs *in vitro*

We used the murine iPSC lines, 959A2-1, 959C1-1, 956F-1 (generous gifts from Dr. Okita and Professor Yamanaka of the Center for iPS Cell Research and Application, Kyoto University, Kyoto, Japan). The cell lines were generated from C57BL/6 (B6) (CLEA) mouse embryonic fibroblasts by introducing *Oct3/4, Sox2, Klf4*, and *c-Myc* without viral vectors as described [19]. The iPSCs were cultured in the absence of serum and feeder cells by using ESGRO Complete PLUS Clonal Grade Medium (Millipore).

Cardiomyogenic differentiation of the iPSCs was performed as described [20,21], with modifications, followed by purification with glucose-free medium supplemented with lactic acid [22]; iPSCs (3×10^3) were resuspended in 100-μL aliquots of differentiation medium [DM; Dulbecco's Modified Eagle's Medium (DMEM; Nacalai Tesque) containing 15% fetal bovine serum (FBS; Biofill), 100 μmol/L non-essential amino acids (NEAA; Invitrogen), 2 mmol/L L-glutamine (Invitrogen), and 0.1 mmol/L 2-mercaptoethanol (Invitrogen)] containing 0.2 μmol/L 6-bromoindirubin-3′-oxime (BIO; a glycogen synthase kinase-3β inhibitor, to activate the Wnt-signaling pathway) (Calbiochem), and cultured in 96-well Corning Costar Ultra-Low attachment multiwell plates (Sigma-Aldrich) for 3 days. On day 3, an additional 100 μL DM without BIO was added to each well. On day 5, individual embryoid bodies (EBs) were transferred to 100-mm gelatin-coated dishes (250 EBs per dish). On days 6, 7, 10, 11, 14, and 15 the medium was exchanged for serum-free Modified Eagle's Medium (MEM; Invitrogen) with insulin transferrin-selenium-X (Invitrogen). On days 8, 9, 12, and 13, the medium was exchanged for Glucose-free DMEM (no glucose, no pyruvate, Invitrogen) supplemented with 4 mmol/L lactic acid (Wako Pure Chemical) for purification of cardiomyocytes. On day 16, the contracting cell clusters were used as cardiomyogenically differentiated iPSCs (959A2-1 CMs, 959C1-1 CMs, 956F-1 CMs: iPSC-CMs). The protocol and purification process are illustrated in Figure 1a.

Adult cardiac tissue from B6 mice (CLEA) was used as a control. Male B6 mice (8 weeks old) were sacrificed by intravenous administration of potassium chloride under inhalation anesthesia of isoflurane, and heart tissue from the left ventricle was harvested for further studies and labeled "Heart".

Immunohistochemistry analysis

IPSC-CMs were dissociated with 0.25% trypsin-EDTA and then fixed with 4% paraformaldehyde. The cells were stained with the following primary antibodies: mouse anti-α-actinin antibody (Sigma-Aldrich) and rabbit anti-troponin I antibody (Abcam), and then visualized by the following secondary antibodies: Alexa Fluor 488 donkey anti-mouse IgG (Invitrogen) and Alexa Fluor 594 goat anti-rabbit IgG (Invitrogen). The nucleus of the cells were stained with 4′, 6-Diamidino-2-phenylindole dihydrochloride (DAPI) and then observed with a confocal laser scanning microscopy FV1200 (Olympus).

Ca^{2+} transient measurement and pharmacological analysis

5 μM Fluo-8 regents (AAT Bioquest, Inc.) in serum-free MEM was added to iPSC-CMs after the cells were washed with phosphate buffered saline. The cells were incubated at 37°C for 30 min and then observed with a fluorescence microscopy. Fluorescence intensity of Fluo-8 dye was sequentially measured using iQ2 software (ANDOR) pre and post the administration of 1 μM isoproterenol.

Flow cytometry

IPSC-CMs were dissociated with 0.25% trypsin-EDTA and then fixed with CytoFix fixation buffer (BD) for 20 min. The cells were permeabilized with Perm/Wash buffer (BD) at room temperature for 10 min and then incubated with mouse anti-troponin T antibody (Thermo) for 30 min. Cells were washed with Perm/Wash buffer prior to incubation with the Alexa Fluor 488 rabbit anti-mouse IgG secondary antibody (Invitrogen) at room temperature for 30 min. These cells were analyzed on a FACS Canto II (BD).

Characterization of *N*-glycans derived from iPSCs, iPSC-CM, and Heart

All experimental procedures, including chromatography conditions and glycosidase treatments, have been described previously [23]. Cultured undifferentiated iPSCs, iPSC-CMs, and the heart tissue were treated with chloroform–methanol, then subjected to proteolysis with chymotrypsin and trypsin, followed by glycoamidase A digestion to release *N*-glycans. After removal of peptides, the reducing ends of the *N*-glycans were derivatized with 2-aminopyridine (Wako). This mixture was applied to a diethylaminoethyl (DEAE) column (Tosoh) or a TSK-gel Amide-80 column (Tosoh); each fraction from the amide column was then applied to a Shim-pack HRC-octadecyl silane (ODS) column (Shimadzu). The elution times of individual peaks from the amide-silica and ODS columns were normalized to a pyridylamino (PA)-derivatized isomalto-oligosaccharide with a known degree of polymerization, and are represented as glucose units (GU). Thus, each compound from these two columns provided a unique set of GU values, which corresponded to the coordinates of the 2D HPLC map. The PA-oligosaccharides were identified by comparison to the coordinates of ~500 reference PA-oligosaccharides in a homemade web application, GALAXY (http://www.glycoanalysis.info/galaxy2/ENG/index.jsp) [24]. The calculated HPLC map based on the unit contribution values was used to estimate some high-mannose type PA-oligosaccharides. The PA-oligosaccharides were co-chromatographed with the reference to PA-oligosaccharides on the columns to confirm their identities. PA-glycans that did not correspond to any of the *N*-glycans registered in GALAXY were trimmed by exoglycosidase to produce a series of known glycans [25].

Mass spectrometry

PA-oligosaccharides were analyzed by matrix-assisted laser desorption/ionization time-of-flight mass spectrometric (MALDI-TOF/MS). The matrix solution was prepared as follows: 10 mg of 2,5-Dihydroxybenzoic acid (Sigma) was dissolved in 1:1 (v/v)

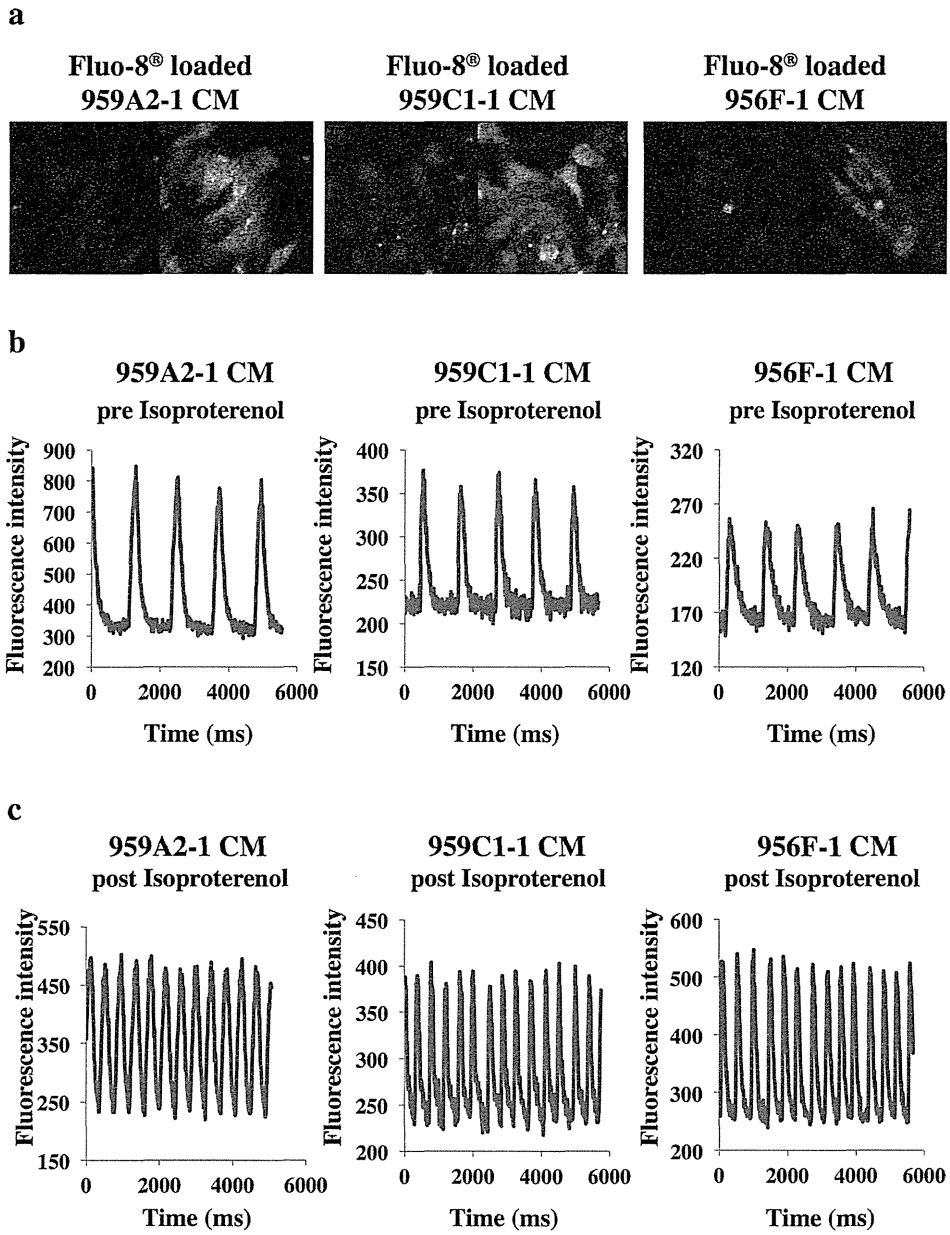

Figure 3. Ca^{2+} transient measurement of iPSC-CMs pre and post the administration of isoproterenol. (a) Fluo-8 loaded iPSC-CMs at the time of low (left) and high (right) fluorescence. (b), (c) Sequentially measured fluorescence intensity of Fluo-8 loaded iPSC-CMs pre (b) and post (c) the administration of 1 μM isoproterenol.
doi:10.1371/journal.pone.0111064.g003

acetonitrile/water (1 mL). Stock solutions of PA-glycans were prepared by dissolving them in pure water. One microliter of a sample solution was mixed on the target spot of a plate with 1 μL matrix solution and then allowed to air-dry. MALDI-TOF/MS data were acquired in the positive mode on an AXIMA-CFR (Shimadzu) operated in linear mode.

Materials

Glycoamidase A from sweet almond, α-mannosidase, β-galactosidase, and β-*N*-acetylhexosaminidase from jack bean were purchased from Seikagaku Kogyo (Tokyo, Japan). α-Galactosidase from coffee bean was purchased from Oxford GlycoSciences (Oxford, UK). Trypsin and chymotrypsin were obtained from Sigma (St. Louis, MO). Pronase protease from *Streptomyces griseus* was from Calbiochem (San Diego, CA). The pyridylamino (PA) derivatives of isomalto-oligosaccharides 4–20 (indicating the degree of polymerization of glucose residues) and reference PA-oligosaccharides were purchased from Seikagaku Kogyo.

Semi-quantitative PCR

DNA-free total RNA was extracted with the RNeasy RNA isolation Kit (Qiagen) and reverse-transcribed into cDNA using Omniscript reverse transcriptase (Qiagen), then analyzed by quantitative real-time PCR on an ABI PRISM 7700 thermocycler (Applied Biosystems) with the following TaqMan gene expression assays (Applied Biosystems): ST3Gal-III (Gal β1-3(4) GlcNAc α-2,

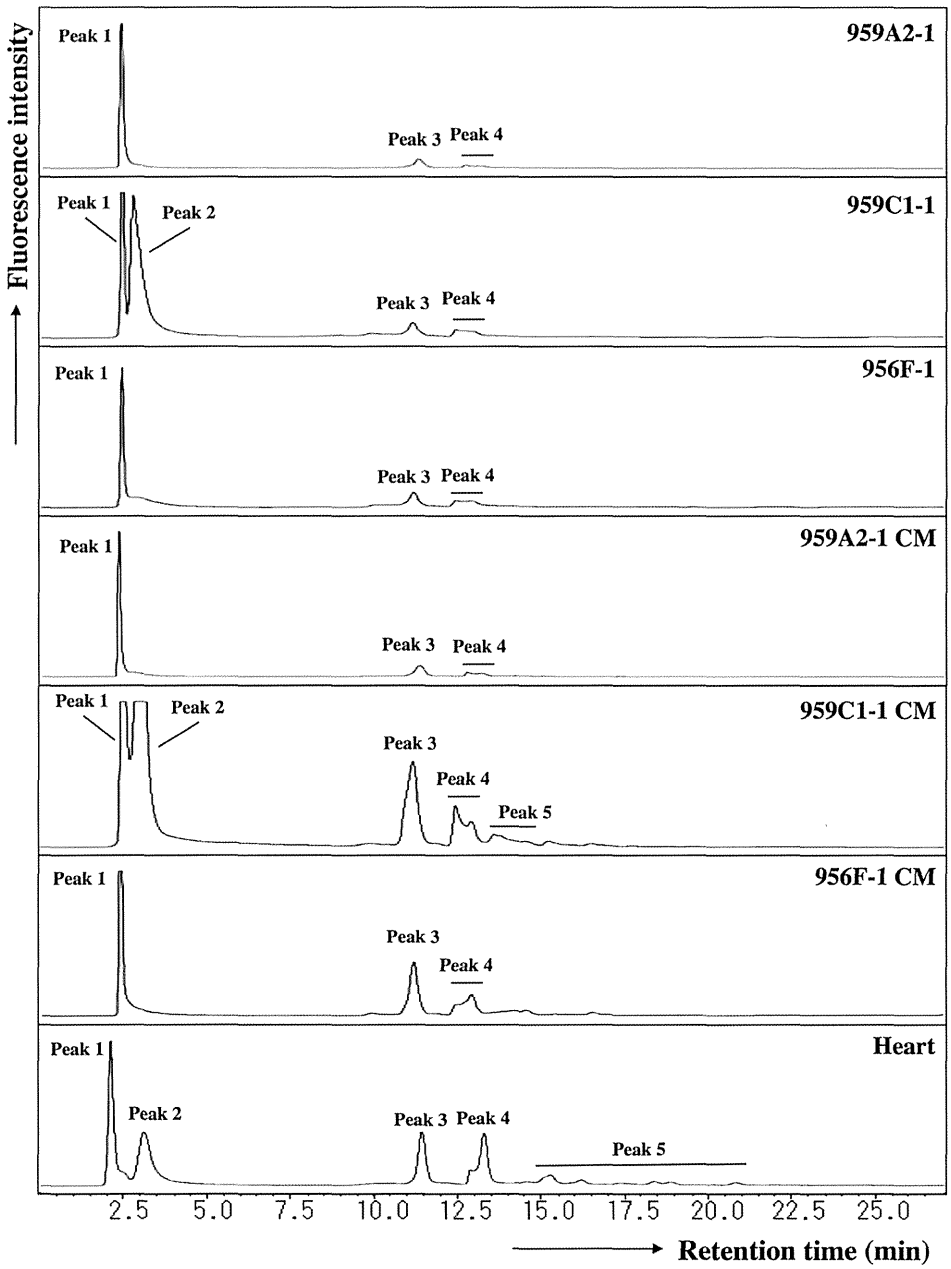

Figure 4. Anion-exchange DEAE elution profiles of PA-glycans. PA-glycans were fractionated according to their sialic acid content as neutral (peak 1), monosialyl (peak 3), and disialyl (peak 4) oligosaccharide fractions. Peaks 2 and 5 represent fractions containing no detectable PA-oligosaccharides.
doi:10.1371/journal.pone.0111064.g004

3-sialyltransferase), Mm00493353_m1; ST4Gal-IV (Gal β1-4(3) GlcNAc α-2, 3-sialyltransferase), Mm00501503_m1; ST6Gal-I (Gal β1-4 GlcNAc α-2, 6-sialyltransferase), Mm00486119_m1; CMAH (cytidine monophosphate-*N*-acetylneuraminic acid hydroxylase), Mm00483341_m1; GAPDH (glyceraldehyde-3-phosphate dehydrogenase), and Mm03302249_g1 and with SYBR Green dye (Applied Biosystems) using the following primers: Nkx2.5 F, 5′- CAAGTGCTCTCCTGCTTTCC -3′ R, 5′- GGCTTTGTCCAGCTCCACT -3′; αMHC (α-myosin heavy chain) F, 5′- GAGATTTCTCCAACCCAG -3′ R, 5′- TCTGACTTTCGGAGGTACT-3′; ANP (atrial natriuretic peptide) F, 5′-AAAGAAACCAGAGTGGGCAGAG -3′ R, 5′- CCAGGGTGATGGAGAAGGAG -3′; Isl1 F, 5′- TTTCCCTGTGTGTTGGTTGC -3′ R, 5′- TGATTACACTCCGCACATTTCA -3′; GAPDH F, 5′- CCAGTATGACTCCACTCACG -3′ R, 5′- GACTCCACGACATACTCAGC -3′. All experiments were performed by the relative standard curve method in three independent, triplicate experiments. Statistical comparison of the data was performed by Student's t-test.

Results

Highly purified cardiomyocytes derived from iPSCs

Cardiomyogenic differentiation was induced in murine iPSCs by using a slightly modified culture protocol (Figure 1a). The iPSC-CMs showed significantly higher expressions of Nkx2.5,

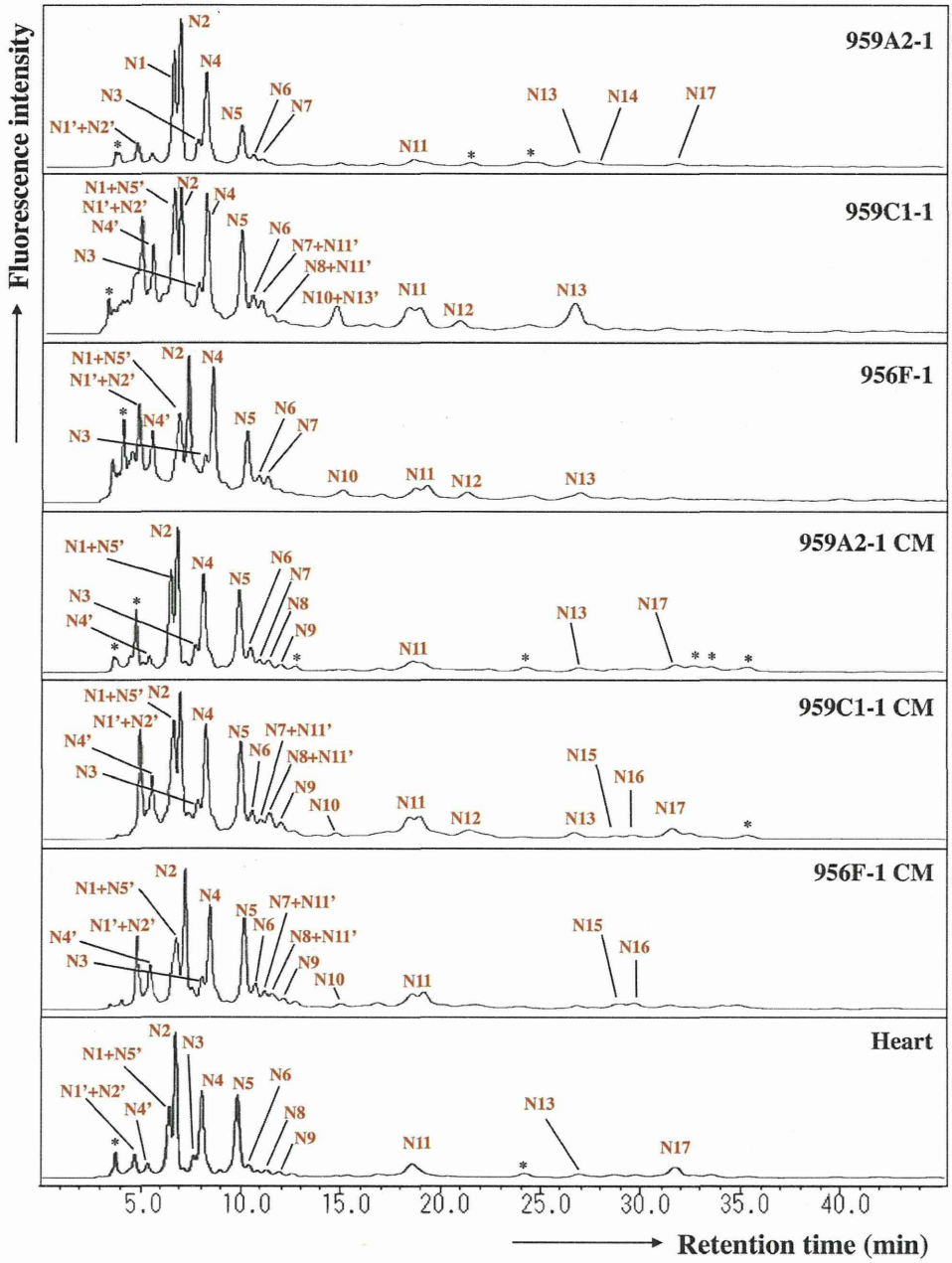

Figure 5. Reverse-phase ODS elution profiles of the neutral PA-glycans. The neutral fractions were individually applied to the ODS column and eluted according to their hydrophobicity. N1′, N2′, N4′, N5′ and N11′: epimerization of N1, N2, N4, N5 and N11. *Fractions containing no detectable PA-oligosaccharides.
doi:10.1371/journal.pone.0111064.g005

αMHC, ANP and Isl1 than undifferentiated iPSCs by semi-quantitative real-time PCR (Figure 2a), and showed sarcomere structures observed by immunohistological staining of α-actinin and troponin I (Figure 1b). The iPSC-CMs were functional with Ca^{2+} transient measurement (Figure 3a, b) and their beating rates were increased by the administration of isoproterenol (Figure 3c), meaning they had β-adrenergic receptors. Nearly all of the iPSC-CMs exhibited spontaneous and regular beating at room temperature (Video S1). The differentiation efficiency of murine iPSC was evaluated by flow cytometry analysis. More than 95% of the 959A2-1 CMs, 92% of the 959C1-1 CMs and 90% of the 956F-1 CMs were positive for troponin T (Figure 2b), while the undifferentiated iPSCs rarely expressed troponin T (Figure 2b).

N-Glycans isolated from iPSCs, iPSC-CM, and Heart

N-glycans extracted from undifferentiated iPSCs (959A2-1: 26 mg, 959C1-1: 11 mg and 956F-1: 10 mg of protein), iPSC-CM (959A2-1 CM: 15 mg, 959C1-1 CM: 12 mg and 956F-1 CM: 5.5 mg of protein), and the B6 heart muscle (82 mg of protein) were separated on a diethylaminoethyl (DEAE) column into five peaks, based on increasing acidity. Peak 1 represented a neutral (N) fraction, peak 3 a monosialyl (M) fraction, and peak 4 a disialyl

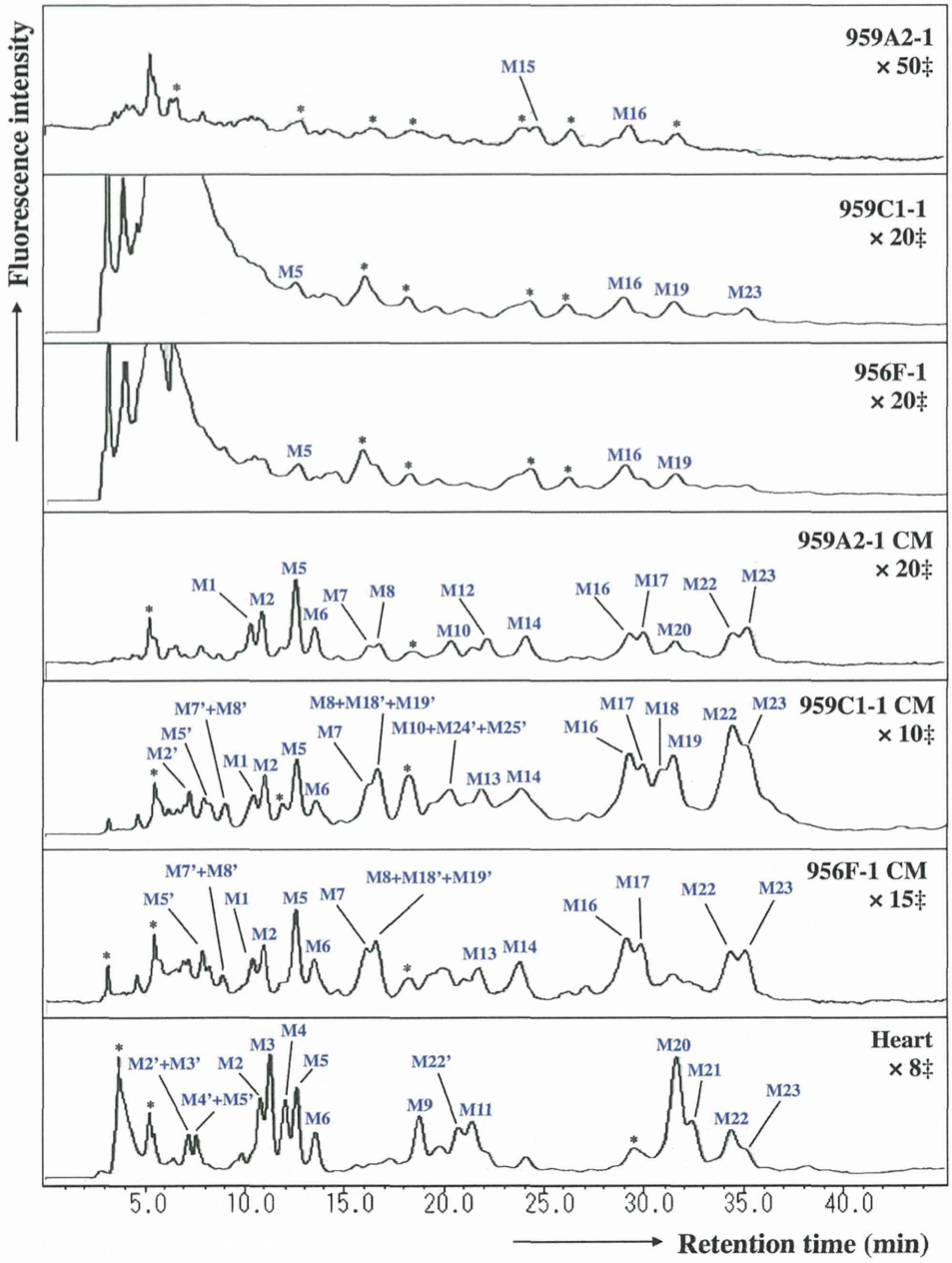

Figure 6. Reverse-phase ODS elution profiles of monosialyl PA-glycans. The monosialyl fractions were individually applied to the ODS column and eluted according to their hydrophobicity. M2′, M3′, M4′, M5′, M7′, M8′, M18′, M19′, M22′, M24′ and M25′: epimerization of M2, M3, M4, M5, M7, M8, M18, M19, M22, M24 and M25. *Fractions containing no detectable PA-oligosaccharides. ‡Magnification ratio to the fluorescence intensity of asialoglycan of each sample.
doi:10.1371/journal.pone.0111064.g006

(D) fraction. Glycan fractions in each of these peaks were as follows: iPSCs yielded 97% N, 0.5% M, 2.6% D (959A2-1), 98% N, 0.7% M, 1.1% D (959C1-1) and 96% N, 1.1% M, 3.1% D (956F-1) peak areas, iPSC-CMs yielded 89% N, 6.4% M, 4.4% D (959A2-1 CM), 79% N, 16% M, 4.8% D (959C1-1 CM) and 82% N, 10% M, 7.9% D (956F-1 CM) and Heart yielded 55% N, 19% M, and 25% D (Figure 4).

The ODS column separated the neutral fraction (Peak 1) into fractions N1–N17 (Figure 5), the monosialyl fraction (Peak 3) into fractions M1–M23 (Figure 6), and the disialyl fraction (Peak 4) into fractions D1–D12 (Figure 7). The signatures of each fraction differed between groups. These ODS fractions were individually fractionated on an amide column and analyzed by MALDI-TOF/MS. The N2, M6, M11, M14, M20, D4, D5, and D10 fractions contained two types of *N*-glycans, and the N6, N9, N11 and M2 fractions three types (data not shown). Thus, 68 different *N*-glycans were isolated from iPSCs, iPSC-CMs, and Heart.

Structures of *N*-Glycans isolated from iPSCs, iPSC-CM, and Heart

The isolated *N*-glycans were analyzed by means of a mapping technique based on their HPLC elution positions and MALDI-TOF/

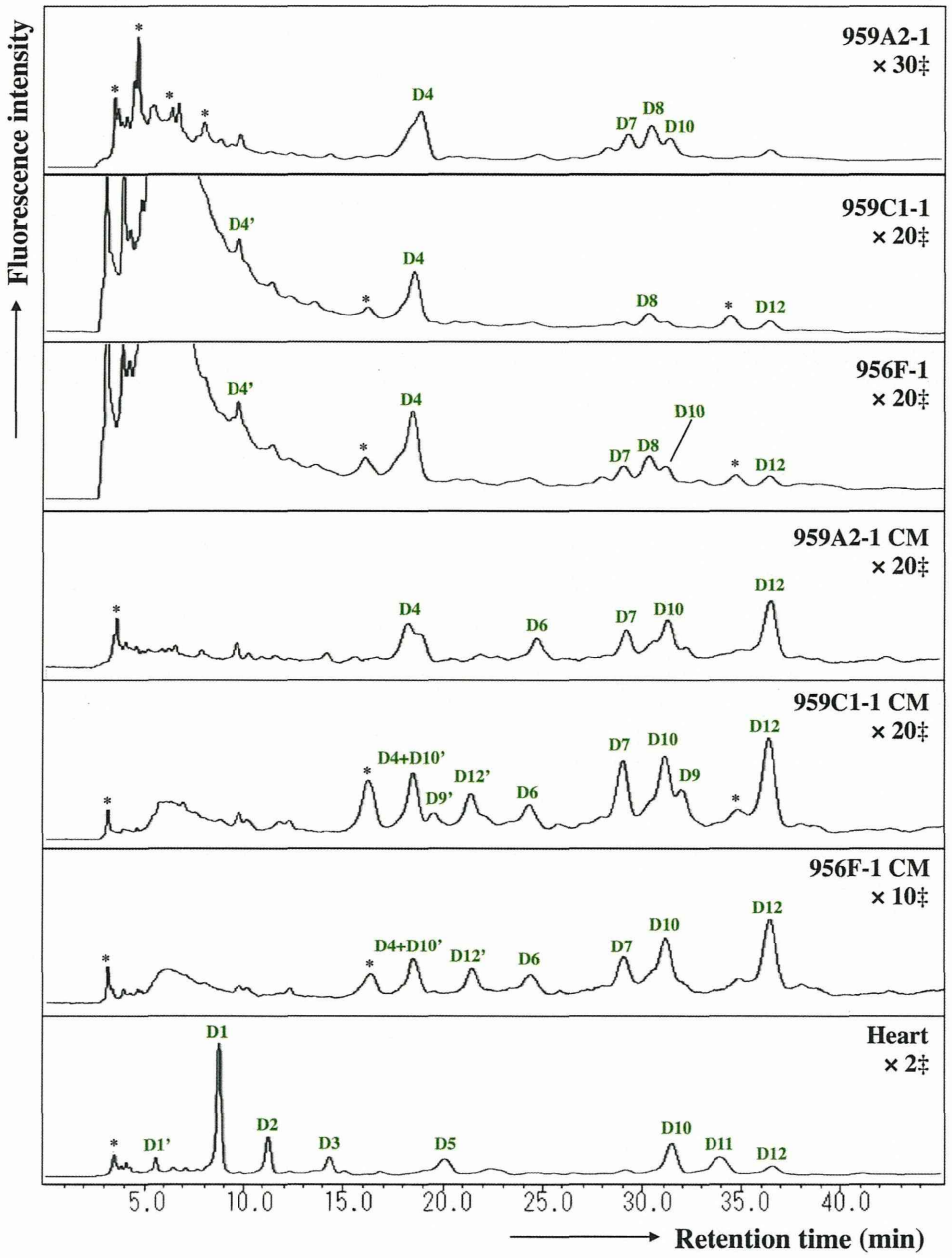

Figure 7. Reverse-phase ODS elution profiles of disialyl PA-glycans. The disialyl fractions were individually applied to the ODS column and eluted according to their hydrophobicity. D1′, D4′, D10′ and D12′: epimerization of D1, D4, D10 and D12; *Fractions containing no detectable PA-oligosaccharides. ‡Magnification ratio to the fluorescence intensity of asialoglycan of each sample.
doi:10.1371/journal.pone.0111064.g007

MS data. The coordinates of 54 *N*-glycans coincided with those for known references in the GALAXY database and their structures were identified. The coordinates for N9-3, M8, M11-2, M12, M13, M15, M17, M18, M19, M20-2, M21, M23, D8 and D9 did not correspond to known references.

N-glycans N9-2, M8, M12, M17, and M23 were trimmed by α-galactosidase but not by β-galactosidase or *N*-acetylglucosamidase. Their structures fit GALAXY references H5.12, 1A1-200.4, 1A3-200.4, 1A1-210.4, and 1A3-210.4, respectively. The galactosyl structures were then identified as Galα1-6Gal, because of the α-galactosidase-driven MS shifts. The structure of the M13 was identified by the coincidence with a GALAXY reference 1A2-H5.12 after being trimmed by α-L-fucosidase. The other *N*-glycans M11-2, M15, M18, M19, M20-2, M21, D8 and D9 were not identified in this study because they did not correspond to GALAXY references even after α-galactosidase digestions. They are described in Figure 8 and Table S1-S5 with their proposed formulas based on MALDI-TOF/MS data.

High-mannose *N*-Glycans were reduced by cardiomyogenic differentiation

The quantity of high-mannose *N*-glycans (HM) calculated from the total volume of N1–N6-2, N7 was highest in the iPSCs (959A2-1: 87.7%, 959C1-1: 68.3% and 956F-1: 78.2%), lower in the

Code No.	N1	N2-1	N2-2	N3	N4	N5	N6-1	N6-2	N6-3	N7	N8	N9-1
GU; ODS (Amid)	5.0 (8.8)	5.3 (7.9)	5.3 (9.5)	6.0 (7.8)	6.2 (7.0)	7.3 (6.0)	7.6 (4.2)	7.6 (5.0)	7.6 (4.6)	7.9 (3.3)	8.1 (7.3)	8.2 (5.6)
Mass (Da)	1800	1638	1962	1638	1475	1313	989	1151	1192	827	1679	1354
Structure	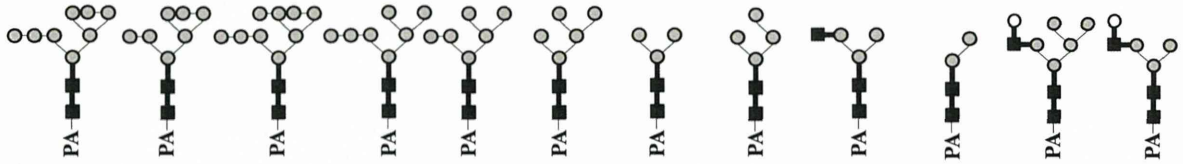											

N9-2	N9-3	N10	N11-1	N11-2	N11-3	N12	N13	N14	N15	N16	N17
8.2 (6.4)	8.3 (8.2)	9.3 (5.0)	10.5 (3.7)	10.5 (4.6)	10.5 (6.9)	11.2 (6.1)	12.8 (5.3)	13.0 (5.0)	13.3 (6.2)	13.5 (6.3)	14.2 (7.3)
1516	1841	1395	973	1135	1720	1500	1541	1338	1704	1704	1866
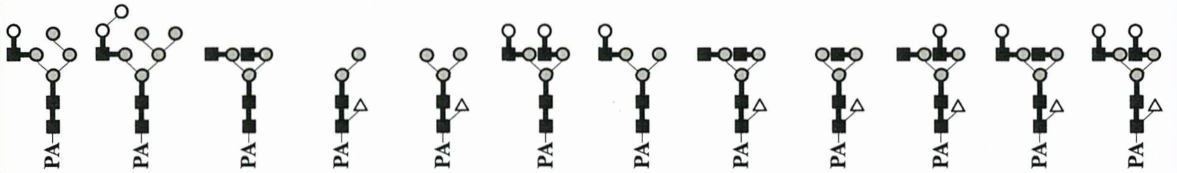											

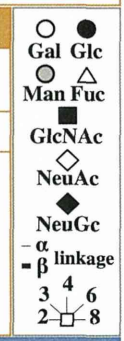

M1	M2-1	M2-2	M2-3	M3	M4	M5	M6-1	M6-2	M7	M8	M9	M10	M11-1	M11-2
7.6 (7.5)	7.9 (5.8)	7.9 (6.6)	7.9 (7.5)	8.1 (7.5)	8.4 (6.7)	8.6 (7.0)	9.0 (5.3)	9.0 (6.1)	10.1 (7.1)	10.3 (7.9)	10.6 (7.1)	11.0 (6.3)	11.3 (6.6)	11.3 (8.8)
1970	1646	1808	2027	1986	1824	1970	1646	1808	2011	2173	2027	1792	2011	2360
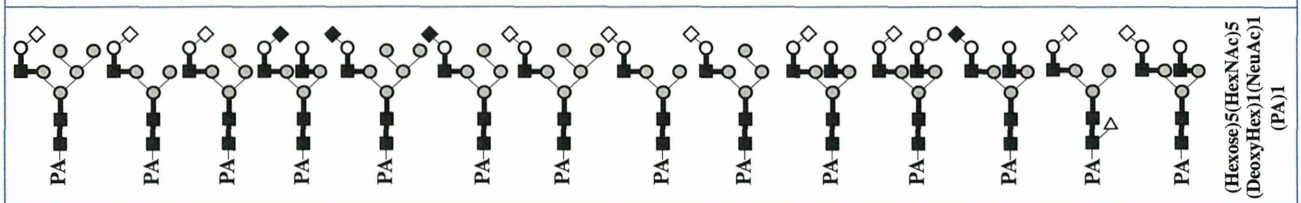														

M12	M13	M14-1	M14-2	M15	M16	M17	M18	M19	M20-1	M20-2	M21	M22	M23
11.5 (7.4)	11.3 (7.4)	11.8 (6.5)	11.8 (5.6)	12.1 (8.3)	13.3 (7.5)	13.7 (8.3)	13.8 (7.4)	14.0 (8.2)	14.2 (7.5)	14.2 (8.2)	14.5 (8.3)	15.1 (6.9)	15.3 (7.8)
2173	2116	1954	1792	2173	2157	2320	2360	2522	2173	2522	2344	2157	2320
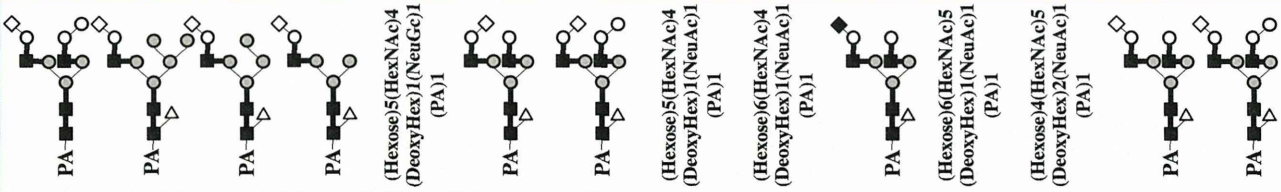													

D1	D2	D3	D4-1	D4-2	D5-1	D5-2	D6	D7	D8	D9	D10-1	D10-2	D11	D12
7.0 (8.2)	8.3 (7.8)	9.3 (8.6)	10.6 (6.9)	10.6 (7.3)	10.9 (7.4)	10.9 (8.1)	12.1 (6.4)	13.5 (7.7)	13.9 (6.8)	14.1 (7.5)	14.2 (7.2)	14.2 (7.7)	15.0 (7.2)	15.9 (6.7)
2334	2334	2480	2302	2302	2334	2480	2302	2448	2537	2854	2448	2480	2464	2448
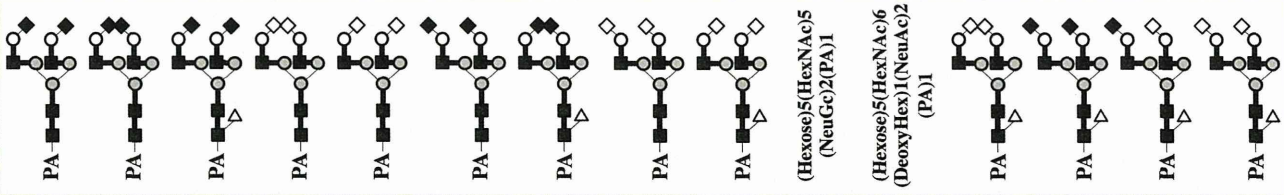														

Figure 8. Structures of neutral, monosialyl, and disialyl PA-oligosaccharides in iPSCs, iPSC-CM, and heart cells. Glucose units (GU) were calculated from the peak elution times for the ODS column in Figure 5, 6 and 7, and the amide column (data not shown). Average mass (Mass) calculated from the *m/z* values of $[M+Na]^+$ or $[M+H]^+$ ion for neutral, $[M-H]^-$ ion for monosialyl, and $[M-H]^-$ & $[M+Na-2H]^-$ ions for disialyl PA-oligosaccharides.
doi:10.1371/journal.pone.0111064.g008

iPSC-CMs (959A2-1 CM: 77.4%, 959C1-1 CM: 60.0% and 956F-1 CM: 65.1%), and lowest in the Heart (46.9%). The quantity of monofucosylated, difucosylated, and other types of *N*-glycans were greater in the iPSC-CMs and Heart (Figure 8, 9).

Sialyl *N*-glycans increased with cardiomyogenic differentiation

The quantity of monosialyl *N*-glycans (MS) calculated from the total volume of M1–M23 increased in iPSC-CMs (959A2-1 CM: 6.4%, 959C1-1 CM: 15.7% and 956F-1 CM: 10.5%) and Heart (19%) and were low in iPSCs (959A2-1: 0.5%, 959C1-1: 0.7% and 956F-1: 1.1%). The disialyl *N*-glycans (DS; D1–D12) yielded a similar pattern. The quantity of asialyl *N*-glycans (AS; N1–N17) decreased in iPSC-CMs (959A2-1 CM: 89.2%, 959C1-1 CM: 79.4% and 956F-1 CM: 81.7%) and Heart (55.3%) in comparison to the iPSCs (959A2-1: 96.9%, 959C1-1: 98.1% and 956F-1: 95.8%) (Figure 9, 10).

Rarely expressed *N*-glycans

The sialic acids identified in this study were either *N*-acetyl neuraminic acid (NeuAc) or *N*-glycolyl neuraminic acid (NeuGc). The quantity of monosialyl and disialyl *N*-glycans containing only NeuAc (A, A/A) was lowest in iPSCs (959A2-1: 2.5%, 959C1-1: 1.7% and 956F-1: 3.7%) and similar in iPSC-CMs (959A2-1 CM: 10.6%, 959C1-1 CM: 21% and 956F-1 CM: 18%) and the Heart (8%). The quantity of monosialyl and disialyl *N*-glycans containing only NeuGc (G, G/G) was markedly higher in the Heart (32.8%) than in iPSCs (959A2-1: 0.6%, 959C1-1: 0.1% and 956F-1: 0.5%) or iPSC-CMs (959A2-1 CM: 0%, 959C1-1 CM: 0% and 956F-1 CM: 0%) (Figure 10a).

Expression of glycosyl transferase, ST3Gal-III, ST3Gal-IV, ST6Gal-I, and CMAH in the iPSCs, iPSC-CMs, and Heart was assessed by RT-PCR to explore the glycan structures responsible for the differences between groups. The Heart expressed high levels of CMAH (0.91±0.13/GAPDH); levels in the iPSCs and iPSC-CMs were markedly lower (iPSCs: 959A2-1 0.011±0.0065/GAPDH, 959C1-1 0.013±0.0070/GAPDH, 956F-1 0.0045±0.0042/GAPDH, $P<0.05$; iPSC-CM: 959A2-1 CM 0.21±0.16/GAPDH, 959C1-1 CM 0.19±0.04, 956F-1 CM 0.45±0.31, $P<0.05$). Expression of ST3Gal-III was significantly higher in the Heart (0.98±0.13/GAPDH) than in iPSCs (959A2-1: 0.21±0.05/GAPDH, 959C1-1: 0.18±0.07/GAPDH, 956F-1: 0.27±0.05/GAPDH) and iPSC-CMs (959A2-1 CM: 0.40±0.10/GAPDH, 959C1-1 CM: 0.35±0.09/GAPDH, 956F-1 CM: 0.66±0.18); expression of ST3Gal-IV did not differ between groups. ST6Gal-I expression was significantly higher in iPSC-CMs (959A2-1 CM: 1.87±0.41/GAPDH, 959C1-1 CM: 1.95±0.22/GAPDH, 956F-1 CM: 3.08±1.27/GAPDH) than in iPSCs (959A2-1: 0.51±0.18/GAPDH, 959C1-1: 0.40±0.09/GAPDH, 956F-1: 0.62±0.29/GAPDH) and the Heart (1.04±0.13/GAPDH) (Figure 10b).

Discussion

Sixty-eight different *N*-glycans were isolated from iPSCs, iPSC-CMs, and the Heart. The structures of 60 *N*-glycans were identified, based on their HPLC elution peaks (Figure 8, Table S1-S5). Each preparation contained a combination of neutral, monosialyl, and disialyl *N*-glycans.

The molar ratios of high-mannose, monofucosylated, and difucosylated *N*-glycans were substantially different between groups (Figure 9), although no clear differences in the abundance of these glycans were found. The decrease in high-mannose *N*-glycans and increase of fucosylated *N*-glycans in iPSC-CMs versus iPSCs is consistent with a previous report on a comparison of ESC derived cardiomyocytes to undifferentiated ESCs [18]. Generally, all *N*-glycans are synthesized from the high-mannose type by a large array of sequentially and competitively acting biosynthetic enzymes located throughout the endoplasmic reticulum and Golgi apparatus [26], indicating that the high-mannose type of *N*-glycans could be categorized as a marker of immaturity. In this study, the high-mannose *N*-glycans were highest in the immature iPSC and lowest in the Heart, or mature tissue; thus, the quantity of high-mannose-type *N*-glycans might be an indicator of maturity in iPSC-derivatives and the iPSC-CMs in our protocol may still be immature in comparison to cardiac tissue.

Clear differences in glycan abundance were observed, such as hybrid and complex types represented by N9-1, N9-3, N15, N16, M1, M2-1, M2-2, M7, M8, M10, M12, M13, M14-1, M14-2, M17, M18, M20-2, D6 and D9 in iPSC-CMs, M2-3, M3, M4, M9, M11-1, M11-2, M20-1, M21, D1, D2, D3, D5-1, D5-2, D10-2 and D11 in Heart and N14 and M15 in iPSCs; these may also be indicators of maturation stage. In addition, expression of monosialyl and disialyl *N*-glycans in iPSC-CMs fell between the levels observed in the iPSCs and Heart, as were the molar ratios, indicating that the iPSC-CMs may still be immature stage. While many *N*-glycolyl neuraminic acid (NeuGc) structures were detected in the Heart, iPSCs and iPSC-CMs did not contain NeuGc in their sialyl structures, except for D8. Moreover, the molar ratio of NeuAc was low in iPSCs and iPSC-CMs. This finding is one of the clearest differences between iPSCs or iPSC-CMs and Heart cells.

The proposed spectra-based composition of the D8 glycans in iPSCs was [(Hexose)5(HexNAc)5(NeuGc)2(PA)1], indicating that it contains NeuGc. However, D8 might be quite a rare exception because transcript levels of CMAH, which catalyzes the conversion of NeuAc to NeuGc, was quite low in iPSCs in comparison to the Heart. This data suggests that during the process of reprograming, iPSCs suppress or eliminate CMAH activity. We conclude that iPSCs contain less sialic acid (especially NeuGc) and high-mannose structures are abundant in the *N*-glycans. In contrast, heart cells produce numerous sialyl-*N*-glycans, especially NeuGc. Transcript levels of CMAH tended to increase in iPSC-CMs relative to iPSCs, suggesting cardiomyogenic differentiation may induce expression of CMAH. If the iPSC-CMs could be matured more closely to the Heart by some additional methods of culture, the quantity of high mannose type of *N*-glycans might decrease more closely to the Heart, and might produce *N*-glycans containing NeuGc, followed by the expression of CMAH.

A terminal NeuGc, the Hanganutziu-Deicher (H-D) epitope [27], is widely distributed in the animal kingdom with the exception of humans and chickens. Expression of NeuGc is controlled by CMAH activity. Irie et al. [28] and Chou et al. [29] cloned the cDNA for human CMAH and reported that the *N*-terminal truncation of human CMAH is caused by deletion of Exon 6, a 92-base pair segment in the genomic DNA. Expression of this truncation in the heart eliminates NeuGc in sialyl

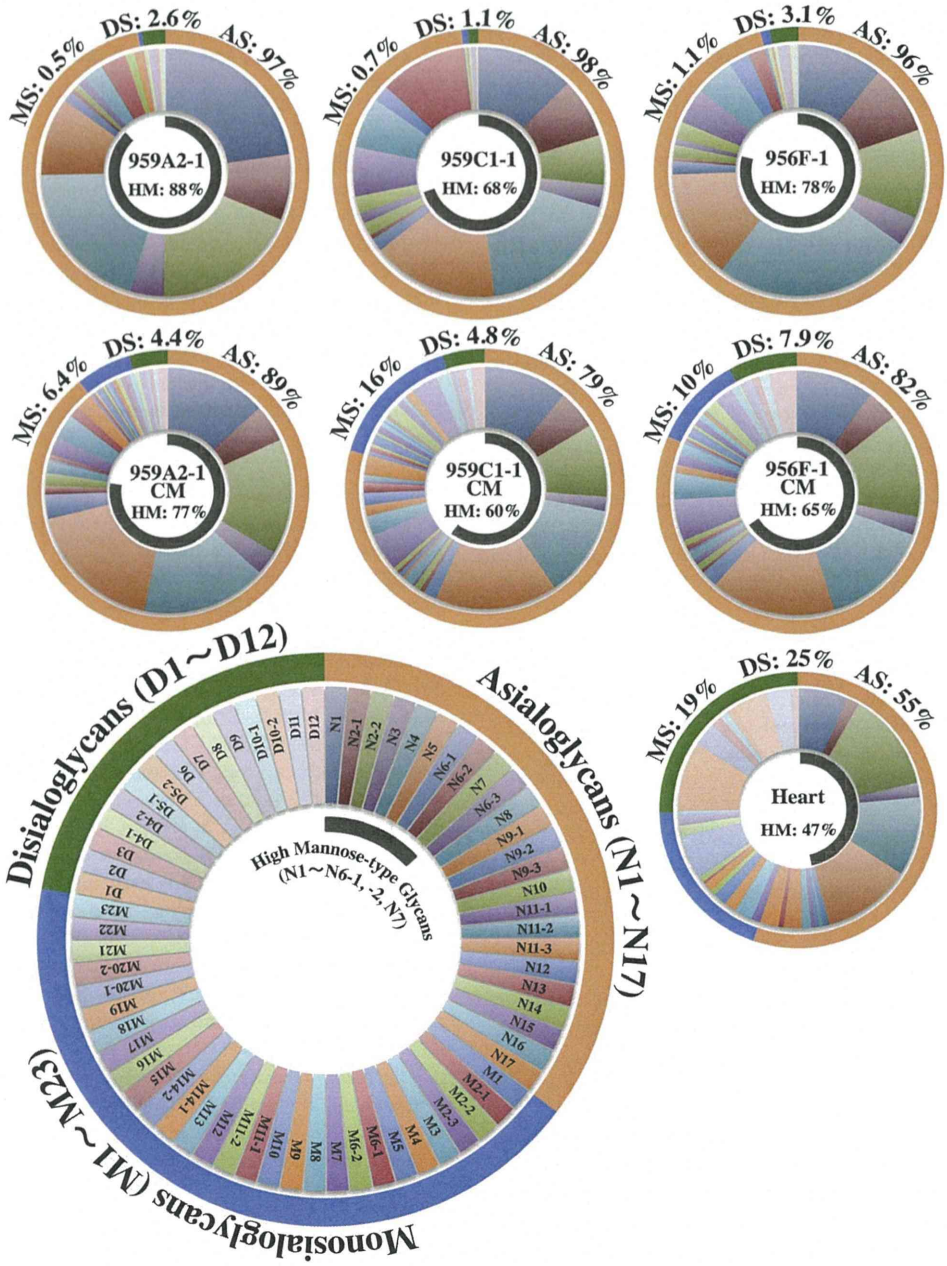

Figure 9. Relative quantities of neutral, monosialyl, and disialyl PA-oligosaccharides in iPSCs, iPSC-CM, and heart cells. Relative quantities of each glycan, calculated from the peak area in Figure 5, 6 and 7 vs. total *N*-glycan content in each cell, were expressed in the doughnut charts. Relative quantities of the asialoglycans, the monosialoglycans and the disialoglycans were showed outside of the charts, and relative quantities of the high mannose type glycans were showed inside of the charts. Asialoglycan (AS): the total volume of N1-N17; Monosialoglycan (MS): the total volume of M1-M23; Disialoglycan (DS): the total volume of D1-D12, High mannose-type glycan (HM): the total volume of N1–N6-1, N6-2, N7.
doi:10.1371/journal.pone.0111064.g009

structures. If human iPSCs or iPSC-CMs do not express CMAH in the same way as murine iPSCs or iPSC-CMs, there may be no difference between human iPSCs, iPSC-CMs, and the human Heart. Further study on human iPSC-CM will be needed to completely understand the features of the sialyl acid of *N*-glycans.

It was reported that human iPSCs produced α2,6sialyl glycans but did not contain α2,3sialyl structures, in contrast to human fibroblast, the origin of iPSCs, which produced α2,3sialyl but not α2,6sialyl structures [30,31]. The murine iPSCs in this study contained α2,3sialyl structures in NeuAc, M5, M23, D4-1, D10-1 and D12, and the iPSC-CMs produced α2,3 and α2,6sialyl structures in NeuAc. These differences may be due to variations between species, because mouse Heart cells also contained α2,3 and α2,6sialyl structures in NeuGc. Further studies are needed to characterize the glycome shift in the production and differentiation of iPSCs.

Type I Lactose structures were not detected, although over 98% of glycans in each cell were accounted for in this study. The *N*-glycans of N9-3, M8, M12, M17, and M23, which were identified after α-galactosidase digestion, contained Galα1-6Gal, not only in

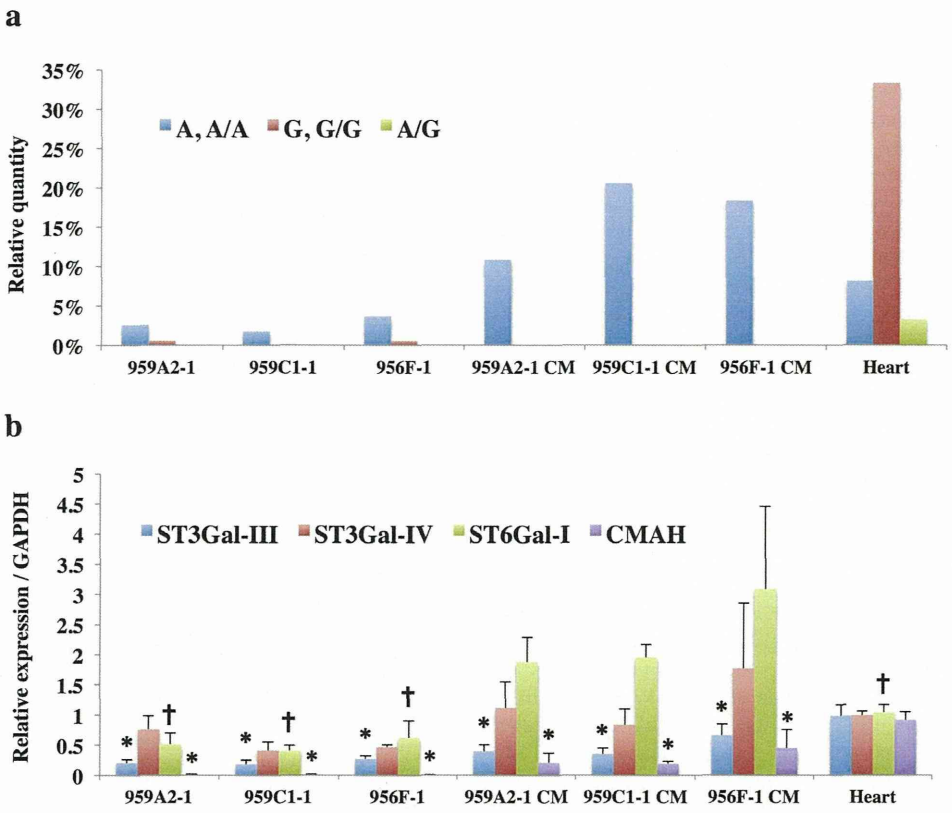

Figure 10. Rarely expressed NeuGc-containing glycans in iPSCs and iPSC-CMs. (a) Relative quantities of NeuAc- and NeuGc-containing glycans; Monosialoglycans containing NeuAc and Disialoglycans containing two NeuAc (A, A/A): the total volume of M1, M2-1, M2-2, M5-M8, M10-M14, M16-M19, M20-2, M21-M23, D4-1, D4-2, D6, D7, D9, D10-1, D12, Disialoglycan containing NeuAc and NeuGc (A/G): D11, Monosialoglycan containing NeuGc and Disialoglycan containing two NeuGc (G, G/G): the total volume of M2-3, M3, M4, M9, M15, M20-1, D1-D3, D5-1, D5-2, D8, D10-2. (b) Transcript expression of ST3Gal-III, ST3Gal-IV, ST6Gal-I, and CMAH; Transcript expression of glycosyltransferases in iPSCs, iPSC-CM, and heart cells was analyzed by real-time PCR. Results are expressed as the mean ± standard deviation. *P<0.05 vs. Heart, †P<0.05 vs. iPSC-CM (all of the 959A2-1 CM, 959C1-1 CM and 956F-1 CM).
doi:10.1371/journal.pone.0111064.g010

the neutral glycans but also in the monosialyl *N*-glycans of the iPSC-CM preparation. The same structure was not found in iPSCs, but only one structure, M23, was present in Heart cells. Therefore, in iPSC-CMs, Galα1-6Gal enzyme activity appears to be up-regulated in comparison to wild-type myocardium, although enzyme activity was not assessed by RT-PCR because of the limited availability of genetic sequence data.

The D8 was identified in all of three iPSC lines and not in the iPSC-CMs and Heart. This structure, unfortunately not identified in this study, may be useful as markers of undifferentiated iPSCs in the same way as well-known pluripotency biomarkers such as stage-specific embryonic antigens (SSEA)-3, SSEA-4 (glycosphingolipids) [32].

Previous MALDI-TOF/MS and MS/MS studies concluded that many kinds of *N*-glycans are found in organs and cells. The number of detected *N*-glycans is attributed to the sensitivity of the MS and HPLC methods employed. That is, MS data are sensitive and can be rapidly obtained, but a glycan structure is identified based only on the calculated molecular weight. Therefore, discriminating between isomeric structures is difficult. On the other hand, it thus appears that the accuracy of the data presented here using HPLC mapping in conjunction with a MALDI-TOF technique provides much more detailed information. Our data were used to identify the representative features of each *N*-glycan in these three cell types.

There may be a concern that the heart tissue used in this study contains connective tissues, vessels or nerves other than cardiomyocytes. Therefore, some of the *N*-glycans detected from the Heart sample might be derived from the tissues other than cardiomyocytes. However, heart is majority composed by cardiomyocytes, and furthermore, even if a small amount of *N*-glycans derived from connective tissues were contaminated in the Heart sample, the main evidences in this study, such as the proportion of the high-mannose type *N*-glycans, the ratio of the active sialyltransferase genes, the existence of NeuGc, and the uncommonness of Galα1-6 Gal, are essentially not affected.

In summary, murine iPSCs were rich in high-mannose type *N*-glycans but very poor in sialyl type *N*-glycans. Murine heart tissue contained a relatively low volume of high-mannose glycans, but was very rich in neuraminic acid, especially NeuGc type sialyl structures. Under these conditions, the volume of each type of glycan was similar for iPSC-CMs and iPSCs. That is, they were rich in high-mannose and relatively poor in sialyl type *N*-glycans by volume. In addition, most of the sialyl structures of the iPSC-CMs were different from those of the Heart, and the iPSC-CMs expressed no NeuGc. Moreover, the iPSC-CMs produced several unique glycans with the Galα1-6Gal structure. These results

provide important data that can be useful in future clinical iPSC studies.

It is quite important to investigate the meaning of *N*-glycans transitions during the cardiomyogenic differentiation presented in this study, for deeply understanding the relationship between the *N*-glycan expression and cardiomyogenic differentiation. Knock-out or knock-down of the genes related to cardiomyogenic differentiation or glycosylation may be useful for such purpose. However, the *N*-glycan signature in the cell surface is determined by a variety of the genes. Knock-out or knock-down of a single gene related to cardiomyogenic differentiation would alter an array of gene expressions, such as sarcomere proteins, transcriptional factors, or cell surface proteins, all of which would affect the signature of *N*-glycans in the cell surface. Therefore, the data interpretation for relationship between expression of a single gene and *N*-glycan signature would be difficult. Some different experimental approach may be needed to investigate the meaning of change in *N*-glycan expression during cardiomyogenic differentiation.

Supporting Information

Table S1 Structures and relative quantities of neutral (Table S1, S2) PA-oligosaccharides derived from iPSC, iPSC-CM, and heart cells. a. Glucose units (GU) were calculated from the peak elution times of the peaks obtained from the ODS column in Figure 5, 6, 7 and the Amide column (data not shown). b. Average mass calculated from the *mlz* values of $[M+Na]^+$ or $[M+H]^+$ ion for neutral, $[M-H]^-$ ion for mono-sialyl, and $[M-H]^-$ & $[M+Na-2H]^-$ ions for di-sialyl PA-oligosaccharides. c. PA-oligosaccharide structures. d. mol% was calculated from the peak area versus total *N*-glycan content in each cell
(TIFF)

Table S2 Structures and relative quantities of neutral (Table S1, S2) PA-oligosaccharides derived from iPSC, iPSC-CM, and heart cells.
(TIFF)

Table S3 Structures and relative quantities of mono-sialyl (Table S3, S4) PA-oligosaccharides derived from iPSC, iPSC-CM, and heart cells.
(TIFF)

Table S4 Structures and relative quantities of mono-sialyl (Table S3, S4) PA-oligosaccharides derived from iPSC, iPSC-CM, and heart cells.
(TIFF)

Table S5 Structures and relative quantities of disialyl PA-oligosaccharides derived from iPSC, iPSC-CM, and heart cells.
(TIFF)

Video S1
(MP4)

Acknowledgments

Our deepest appreciation goes to Professor Shinya Yamanaka and Keisuke Okita of the Center for iPS Cell Research and Application, Kyoto University, who kindly provided the murine iPSCs. We also thank Sachiko Kondo and Uichiro Yabe of MBL, Nagoya, Japan, who gave invaluable comments regarding *N*-glycan analysis.

Author Contributions

Conceived and designed the experiments: TK S. Miyagawa S. Miyagawa JL YS. Performed the experiments: TK AY NK AK EI AM HE KT. Analyzed the data: TK S. Miyagawa YS. Contributed reagents/materials/analysis tools: TK AY JL. Wrote the paper: TK S. Miyagawa YS SF. Obtained permission for use of cell line: S. Miyagawa AS YS.

References

1. Gonzales C, Pedrazzini T (2009) Progenitor cell therapy for heart disease. Exp Cell Res 315: 3077–3085.
2. Shah AM, Mann DL (2011) In search of new therapeutic targets and strategies for heart failure: recent advances in basic science. Lancet 378: 704–712.
3. Yoshida Y, Yamanaka S (2010) Recent stem cell advances: induced pluripotent stem cells for disease modeling and stem cell-based regeneration. Circulation 122: 80–87.
4. Yoshida Y, Yamanaka S (2011) iPS cells: A source of cardiac regeneration. Journal of Molecular and Cellular Cardiology 50: 327–332.
5. Kawamura M, Miyagawa S, Miki K, Saito A, Fukushima S, et al. (2012) Feasibility, safety, and therapeutic efficacy of human induced pluripotent stem cell-derived cardiomyocyte sheets in a porcine ischemic cardiomyopathy model. Circulation 126: S29–37.
6. Mercola M, Colas A, Willems E (2013) Induced pluripotent stem cells in cardiovascular drug discovery. Circ Res 112: 534–548.
7. Sinnecker D, Goedel A, Laugwitz KL, Moretti A (2013) Induced pluripotent stem cell-derived cardiomyocytes: a versatile tool for arrhythmia research. Circ Res 112: 961–968.
8. Kamakura T, Makiyama T, Sasaki K, Yoshida Y, Wuriyanghai Y, et al. (2013) Ultrastructural maturation of human-induced pluripotent stem cell-derived cardiomyocytes in a long-term culture. Circ J 77: 1307–1314.
9. Kuzmenkin A, Liang H, Xu G, Pfannkuche K, Eichhorn H, et al. (2009) Functional characterization of cardiomyocytes derived from murine induced pluripotent stem cells in vitro. FASEB J 23: 4168–4180.
10. Varki A (1993) Biological roles of oligosaccharides: all of the theories are correct. Glycobiology 3: 97–130.
11. Haltiwanger RS, Lowe JB (2004) Role of glycosylation in development. Annu Rev Biochem 73: 491–537.
12. Ohtsubo K, Marth JD (2006) Glycosylation in cellular mechanisms of health and disease. Cell 126: 855–867.
13. Surani MA (1979) Glycoprotein synthesis and inhibition of glycosylation by tunicamycin in preimplantation mouse embryos: compaction and trophoblast adhesion. Cell 18: 217–227.
14. Akama TO, Nakagawa H, Sugihara K, Narisawa S, Ohyama C, et al. (2002) Germ cell survival through carbohydrate-mediated interaction with Sertoli cells. Science 295: 124–127.
15. Hato M, Nakagawa H, Kurogochi M, Akama TO, Marth JD, et al. (2006) Unusual N-glycan structures in alpha-mannosidase II/IIx double null embryos identified by a systematic glycomics approach based on two-dimensional LC mapping and matrix-dependent selective fragmentation method in MALDI-TOF/TOF mass spectrometry. Mol Cell Proteomics 5: 2146–2157.
16. Lau KS, Partridge EA, Grigorian A, Silvescu CI, Reinhold VN, et al. (2007) Complex N-glycan number and degree of branching cooperate to regulate cell proliferation and differentiation. Cell 129: 123–134.
17. Kraushaar DC, Rai S, Condac E, Nairn A, Zhang S, et al. (2012) Heparan sulfate facilitates FGF and BMP signaling to drive mesoderm differentiation of mouse embryonic stem cells. J Biol Chem 287: 22691–22700.
18. Amano M, Yamaguchi M, Takegawa Y, Yamashita T, Terashima M, et al. (2010) Threshold in stage-specific embryonic glycotypes uncovered by a full portrait of dynamic N-glycan expression during cell differentiation. Mol Cell Proteomics 9: 523–537.
19. Okita K, Nakagawa M, Hyenjong H, Ichisaka T, Yamanaka S (2008) Generation of mouse induced pluripotent stem cells without viral vectors. Science 322: 949–953.
20. Miki K, Uenaka H, Saito A, Miyagawa S, Sakaguchi T, et al. (2012) Bioengineered myocardium derived from induced pluripotent stem cells improves cardiac function and attenuates cardiac remodeling following chronic myocardial infarction in rats. Stem Cells Transl Med 1: 430–437.
21. Yu T, Miyagawa S, Miki K, Saito A, Fukushima S, et al. (2013) In vivo differentiation of induced pluripotent stem cell-derived cardiomyocytes. Circ J 77: 1297–1306.
22. Tohyama S, Hattori F, Sano M, Hishiki T, Nagahata Y, et al. (2013) Distinct metabolic flow enables large-scale purification of mouse and human pluripotent stem cell-derived cardiomyocytes. Cell Stem Cell 12: 127–137.
23. Takahashi N, Khoo KH, Suzuki N, Johnson JR, Lee YC (2001) N-glycan structures from the major glycoproteins of pigeon egg white: predominance of terminal Galalpha(1)Gal. J Biol Chem 276: 23230–23239.

24. Takahashi N, Kato K (2003) GALAXY(Glycoanalysis by the Three Axes of MS and Chromatography): a Web Application that Assists Structural Analyses of N-Glycans. Trends in Glycoscience and Glycotechnology 15 No.84: 235–251.
25. Yagi H, Takahashi N, Yamaguchi Y, Kimura N, Uchimura K, et al. (2005) Development of structural analysis of sulfated N-glycans by multidimensional high performance liquid chromatography mapping methods. Glycobiology 15: 1051–1060.
26. Dalziel M, Crispin M, Scanlan CN, Zitzmann N, Dwek RA (2014) Emerging principles for the therapeutic exploitation of glycosylation. Science 343: 1235681.
27. Varki A (2009) Multiple changes in sialic acid biology during human evolution. Glycoconj J 26: 231–245.
28. Irie A, Koyama S, Kozutsumi Y, Kawasaki T, Suzuki A (1998) The molecular basis for the absence of N-glycolylneuraminic acid in humans. J Biol Chem 273: 15866–15871.
29. Chou HH, Takematsu H, Diaz S, Iber J, Nickerson E, et al. (1998) A mutation in human CMP-sialic acid hydroxylase occurred after the Homo-Pan divergence. Proc Natl Acad Sci U S A 95: 11751–11756.
30. Hasehira K, Tateno H, Onuma Y, Ito Y, Asashima M, et al. (2012) Structural and quantitative evidence for dynamic glycome shift on production of induced pluripotent stem cells. Mol Cell Proteomics 11: 1913–1923.
31. Tateno H, Toyota M, Saito S, Onuma Y, Ito Y, et al. (2011) Glycome diagnosis of human induced pluripotent stem cells using lectin microarray. J Biol Chem 286: 20345–20353.
32. Fujitani N, Furukawa J, Araki K, Fujioka T, Takegawa Y, et al. (2013) Total cellular glycomics allows characterizing cells and streamlining the discovery process for cellular biomarkers. Proc Natl Acad Sci U S A 110: 2105–2110.

STEM CELLS AND DEVELOPMENT
Volume 23, Number 18, 2014

DOI: 10.1089/scd.2013.0642

Role of Notch Signaling in the Maintenance of Human Mesenchymal Stem Cells Under Hypoxic Conditions

Hiroyuki Moriyama,[1,*] Mariko Moriyama,[1,*] Haruki Isshi,[1] Shin Ishihara,[1] Hanayuki Okura,[2] Akihiro Ichinose,[3] Toshiyuki Ozawa,[4] Akifumi Matsuyama,[2] and Takao Hayakawa[1]

Human adipose tissue-derived multilineage progenitor cells (hADMPCs) are attractive for cell therapy and tissue engineering because of their multipotency and ease of isolation without serial ethical issues. However, their limited in vitro lifespan in culture systems hinders their therapeutic application. Some somatic stem cells, including hADMPCs, are known to be localized in hypoxic regions; thus, hypoxia may be beneficial for ex vivo culture of these stem cells. These cells exhibit a high level of glycolytic metabolism in the presence of high oxygen levels and further increase their glycolysis rate under hypoxia. However, the physiological role of glycolytic activation and its regulatory mechanisms are still incompletely understood. Here, we show that Notch signaling is required for glycolysis regulation under hypoxic conditions. Our results demonstrate that 5% O_2 dramatically increased the glycolysis rate, improved the proliferation efficiency, prevented senescence, and maintained the multipotency of hADMPCs. Intriguingly, these effects were not mediated by hypoxia-inducible factor (HIF), but rather by the Notch signaling pathway. Five percent O_2 significantly increased the level of activated Notch1 and expression of its downstream gene, *HES1*. Furthermore, 5% O_2 markedly increased glucose consumption and lactate production of hADMPCs, which decreased back to normoxic levels on treatment with a γ-secretase inhibitor. We also found that HES1 was involved in induction of GLUT3, TPI, and PGK1 in addition to reduction of TIGAR and SCO2 expression. These results clearly suggest that Notch signaling regulates glycolysis under hypoxic conditions and, thus, likely affects the cell lifespan via glycolysis.

Introduction

HUMAN ADIPOSE TISSUE-DERIVED mesenchymal stem cells (MSCs), also referred to as human adipose tissue-derived multilineage progenitor cells (hADMPCs), are multipotent stem cells that can differentiate into various types of cells, including hepatocytes [1], cardiomyoblasts [2], pancreatic cells [3], and neuronal cells [4–6]. They can be easily and safely obtained from lipoaspirate without posing serious ethical issues and can also be expanded ex vivo under appropriate culture conditions. Moreover, MSCs, including hADMPCs, have the ability to migrate to injured areas and secrete a wide variety of cytokines and growth factors that are necessary for tissue regeneration [7–11]. In addition, due to their hypoimmunogenicity and immunomodulatory effects, hADMPCs are good candidates as gene delivery vehicles for therapeutic purposes [12]. Thus, hADMPCs are attractive seeding cells for cell therapy and tissue engineering. However, similar to other somatic stem cells or primary cells, hADMPCs have limited growth potential and ultimately stop proliferation as a result of cellular senescence [13], which hinders their therapeutic application.

Conversely, embryonic stem cells (ESCs) and induced pluripotent stem cells (iPSCs) are immortal under standard culture conditions. Recently, several groups have reported that these cells greatly rely on glycolysis for energy production even under high-oxygen conditions [14–16]. This phenomenon is known as the Warburg effect and was originally described for cancer cells by Otto Warburg in the 1920s [17]. Although mitochondrial respiration is more efficient than glycolysis in generating ATP (net yield of 30 ATPs vs. 2 ATPs), glycolysis is able to produce ATP considerably faster than mitochondrial respiration as long as glucose supplies are adequate. Thus, a metabolic shift from mitochondrial respiration to glycolysis would provide a growth advantage for actively proliferating cells. Moreover, Kondoh et al. demonstrated that enhanced glycolysis is also involved in cellular immortalization through reduction of

[1]Pharmaceutical Research and Technology Institute, Kinki University, Higashi-Osaka, Osaka, Japan.
[2]Platform of Therapeutics for Rare Disease and Health Policy, National Institute of Biomedical Innovation, Kobe, Japan.
[3]Department of Plastic Surgery, Kobe University Hospital, Kobe, Japan.
[4]Department of Dermatology, Graduate School of Medicine, Osaka City University, Osaka, Japan.
*These two authors contributed equally to this work.

intrinsic reactive oxygen species (ROS) production [14,18,19]. Since accumulation of intrinsic ROS levels could be a major reason for replicative senescence [20], enhancing glycolysis in cultured cells might improve the quality of the cells by suppressing premature senescence. One candidate method for induction of glycolysis is application of low-oxygen conditions to activate the transcription factor, hypoxia-inducible factor (HIF). HIF-1 is known to increase the expression of most glycolytic enzymes and the glucose transporters GLUT1 and GLUT3 [20]. Thus, several studies have reported that hypoxia is beneficial for the maintenance of hESCs in a pluripotent state [21,22]. Moreover, low oxygen tension has been reported to enhance the generation of iPSCs both from mouse and human primary fibroblasts [23].

Recently, hypoxic culture conditions have also been reported to confer a growth advantage, prevent premature senescence, and maintain undifferentiated states in somatic stem cells; for example, hematopoietic stem cells (HSCs) [24], neural stem cells [25], and bone marrow-derived MSCs [26]. These stem cells reside in their local microenvironments called the "stem cell niche," where the oxygen tension is relatively low (in the range of 1%–9%). Thus, hypoxic culture may be beneficial to these stem cells with regard to in vitro proliferation, cell survival, and differentiation. Takubo et al. reported that HSCs activated Pdk through HIF1α in hypoxic culture conditions, resulting in maintenance of glycolytic flow and suppression of the influx of glycolytic metabolites into mitochondria, and this glycolytic metabolic state was shown to be indispensable for the maintenance of HSCs [27]. Several studies have reported that MSCs exhibit a high level of glycolytic metabolism in the presence of high oxygen levels and further increase their rate of glycolysis on culture under hypoxia [28,29]. However, a relationship between beneficial effects of hypoxic conditions and metabolic status in addition to involvement of HIFs in the metabolic changes has not been investigated in these reports.

In this study, we aimed at investigating the effect of 5% oxygen on hADMPCs. Our results demonstrate that culture under 5% oxygen increased the glycolysis rate, improved the proliferation efficiency, prevented the cellular senescence, and maintained the undifferentiated status of hADMPCs. Intriguingly, these effects were not mediated by HIF, but rather by Notch signaling, an important signaling pathway required for the development of many cell types and maintenance of stem cells [30,31]. Five percent oxygen activated Notch signaling, resulting in the upregulation of *SLC2A3*, *TPI*, and *PGK1* in addition to the downregulation of *TIGAR* and *SCO2*, which may contribute to the increase in the glycolysis rate. These observations, thus, provide new regulatory mechanisms for stemness maintenance obtained under 5% oxygen conditions.

Materials and Methods

Adipose tissue samples

Subcutaneous adipose tissue samples (10–50 g each) were resected during plastic surgery from five female and two male patients (age 20–60 years) as discarded tissue. The study protocol was approved by the Review Board for Human Research of Kobe University Graduate School of Medicine Foundation for Biomedical Research and Innovation, Osaka City University Graduate School of Medicine, and Kinki University Pharmaceutical Research and Technology Institute (reference number: 12-043). Each subject provided signed informed consent.

Cell culture

hADMPCs were isolated as previously reported [11,32–34] and maintained in a medium containing 60% DMEM low glucose, 40% MCDB-201 medium (Sigma Aldrich), 1× insulin-transferrin-selenium (Life Technologies), 1 nM dexamethasone (Sigma Aldrich), 100 mM ascorbic acid 2-phosphate (Wako), 10 ng/mL epidermal growth factor (PeproTech), and 5% fetal bovine serum. The cells were plated to a density of 5×10^3 cells/cm^2 on fibronectin-coated dishes, and the medium was replaced every 2 days. For hypoxic culture, cells were cultured in a gas mixture composed of 90% N_2, 5% CO_2, and 5% O_2. For maintenance of the hypoxic gas mixture, a ProOx C21 carbon dioxide and oxygen controller and a C-Chamber (Biospherix) were used.

Senescence-associated β-galactosidase staining

Cells were fixed with 2% paraformaldehyde/0.2% glutaradehyde for 5 min at room temperature and then washed twice with phosphate-buffered saline (PBS). The cells were then incubated overnight at 37°C with fresh senescence-associated β-galactosidase (SA-β-Gal) chromogenic substrate solution (1 mg/mL Bluo-gal (Life Technologies), 40 mM citric acid (pH 6.0), 5 mM potassium ferrocyanide, 5 mM potassium ferricyanide, 150 mM NaCl, and 2 mM $MgCl_2$).

Measurement of ROS production

Cells were harvested and incubated with 10 μM 5-(and-6)-chloromethyl-2′,7′-dichlorodihydrofluorescein diacetate, acetyl ester (CM-H_2DCFDA). The amount of intracellular ROS production was proportional to the green fluorescence, as analyzed using a Guava EasyCyte 8HT flow cytometer (Millipore) using an argon laser at 488 nm and a 525/30 nm band pass filter, and dead cells were excluded using the Live/Dead Fixable Far Red Dead Cell Stain Kit (Life Technologies).

EdU proliferation assay

For assessment of cell proliferation, hADMPCs were seeded on a fibronectin-coated six-well plate at a density of 5×10^3 cells/cm^2 and cultured for 3 days. Cell proliferation was detected by incorporating of 5-ethynyl-2′-deoxyuridine (EdU) and using the Click-iT EdU Alexa Fluor 488 Flow Cytometry Assay Kit (Life Technologies). Briefly, according to the manufacturer's protocol, cells were incubated with 10 μM EdU for 2 h before fixation, permeabilized, and stained with EdU. EdU-positive cells were then analyzed using the 488 nm laser of a Guava EasyCyte 8HT flow cytometer (Millipore).

Flow cytometry analysis

Flow cytometry analysis was performed as previously described [34]. Briefly, hADMPCs were harvested and resuspended in staining buffer (PBS containing 1% BSA, 2 mM EDTA, and 0.01% sodium azide) at a density of

1×10^6 cells/mL, incubated for 20 min with a fluorescein isothiocyanate (FITC)-conjugated antibody against CD49b or CD98 (BioLegend) or a phycoerythrin (PE)-conjugated antibody against CD10, CD13, CD29, CD44, CD49a, CD49c, CD49d, CD49e, CD51/61, CD73, CD90, CD105, CD117, SSEA4, HLA-A,B,C (BioLegend), CD133/1 (Miltenyi Biotec), or CD166 (Beckman Coulter). Nonspecific staining was assessed using relevant isotype controls. Dead cells were excluded using the Live/Dead Fixable Far Red Dead Cell Stain Kit (Life Technologies). FlowJo software was used for quantitative analysis.

RNA extraction, cDNA generation, and quantitative polymerase chain reaction

Total RNA was extracted using the RNeasy Mini Kit (Qiagen) accroding to the manufacturer's instructions. cDNA was generated from 1 μg of total RNA using the Verso cDNA Synthesis Kit (Thermo Scientific) and purified using the MinElute PCR Purification Kit (Qiagen). Quantitative polymerase chain reaction (Q-PCR) analysis was conducted using the SsoFast EvaGreen supermix (Bio-Rad) according to the manufacturer's protocols. The relative expression value for each gene was calculated using the ΔΔCt method, and the most reliable internal control gene was determined using geNorm Software (http://medgen.ugent.be/~jvdesomp/genorm/). Details of the primers used in these experiments are available on request.

Western blot analysis

Whole cell extracts were prepared by washing cells with ice-cold PBS and lysing them with M-PER Mammalian Protein Extraction Reagent (Thermo Scientific Pierce) according to the manufacturer's instructions. Nuclear and cytosolic extracts were prepared as follows. Cells were washed with ice-cold PBS and lysed with lysis buffer (50 mM Tris-HCl (pH 7.5), 0.5% Triton X-100, 137.5 mM NaCl, 10% glycerol, 5 mM EDTA, 1 mM sodium vanadate, 50 mM sodium fluoride, 10 mM sodium pyrophosphate, and protease inhibitor cocktail). Then, insoluble nuclei were isolated by centrifugation and lysed with lysis buffer containing 0.5% SDS. Equal amounts of proteins were separated by sodium dodecyl sulfate polyacrylamide gel electrophoresis (SDS-PAGE), transferred to polyvinylidene fluoride membranes (Immobilon-P; Millipore), and probed with antibodies against cleaved Notch1 (#2421; Cell Signaling Technology), HIF-1α (#610959; BD Bioscience), hypoxia-inducible factor 2α (MAB3472; Millipore), Akt (#9272; Cell Signaling Technology), and phospho Akt (Ser473) (#4060; Cell Signaling Technology). Horseradish peroxidase (HRP)-conjugated anti-mouse or -rabbit IgG antibody (Cell Signaling Technology) was used as a secondary antibody, and immunoreactive bands were visualized using Immobilon Western Chemiluminescent HRP substrate (Millipore). The band intensity was measured using the ImageJ software.

Fluorescence microscopy

Phase-contrast and fluorescence images were obtained using a fluorescence microscope (BZ-9000; Keyence) using BZ Analyzer Software (Keyence).

Adipogenic, osteogenic, and chondrogenic differentiation procedures

For adipogenic differentiation, cells were cultured in differentiation medium (Zen-Bio). After 7 days, half of the medium was exchanged for adipocyte medium (Zen-Bio) and this was repeated every 3 days. Three weeks after differentiation, adipogenic differentiation was confirmed by a microscopic observation of intracellular lipid droplets with the aid of Oil Red O staining. Osteogenic differentiation was induced by culturing the cells in osteocyte differentiation medium (Zen-Bio). Differentiation was examined by Alizarin Red staining. For chondrogenic differentiation, 2×10^5 hADMSCs were centrifuged at 400 *g* for 10 min. The resulting pellets were cultured in chondrogenic medium (Lonza) for 21 days. The pellets were fixed with 4% paraformaldehyde in PBS, embedded in OCT, frozen, and sectioned at 8 μm. The sections were incubated with PBSMT (PBS containing 0.1% Triton X-100, and 2% skim milk) for 1 h at room temperature, and then incubated with a mouse monoclonal antibody against type II collagen (Abcam) for 1 h. After washing with PBS, cells were incubated with Alexa 546-conjugated anti-mouse IgG to identify chondrocytes (Life Technologies). The cells were counterstained with 4′-6-diamidino-2-phenylindole (DAPI) (Life Technologies) to identify cellular nuclei. The sections were also stained with 1% alcian blue (Sigma Aldrich) in 3% acetic acid, pH 2.5 for 30 min.

Determination of HK, PFK, LDH, PDH, and Cox IV activities

Cells (2×10^6) were lysed, and HK, PFK, LDH, or PDH activity was measured using the Hexokinase Colorimetric Activity Kit, Phosphofructokinase (PFK) Activity Colorimetric Assay Kit, Lactate Dehydrogenase (LDH) Activity Assay Kit, or Pyruvate Dehydrogenase Activity Colorimetric Assay Kit (all from BioVision), respectively, according to the manufacturer's instructions. To measure Cox IV activity, mitochondria were isolated from 2×10^7 cells using a Mitochondria Isolation Kit (Thermo Scientific) and lysed with buffer containing n-Dodecyl β-D-maltoside, followed by measurement with the Mitochondria Activity Assay (Cytochrome C Oxidase Activity Assay) Kit (BioChain Institute), according to the manufacturer's instructions.

Results

5% oxygen hypoxic culture condition increases proliferation capacity and decreases senescence

hADMPCs were cultured under 20% oxygen (normoxia; Nx) or 5% oxygen (hypoxia; Hx), and their proliferation capacities were examined based on the relationship between the number of cultivation days and the population doubling level (PDL). Nx-cultured hADMPCs ceased proliferation at a PDL of 35–40 (between 46–70 days), whereas continuous cell proliferation beyond 45 PDL was observed when hADMPCs were cultured in the Hx condition (Fig. 1A). To investigate whether this increase of PDL in the Hx culture condition resulted from an increase in cell cycle progression and increase in survival rates, EdU, an alternative to 5-bromo-2′-deoxyuridine (BrdU), was incorporated into the

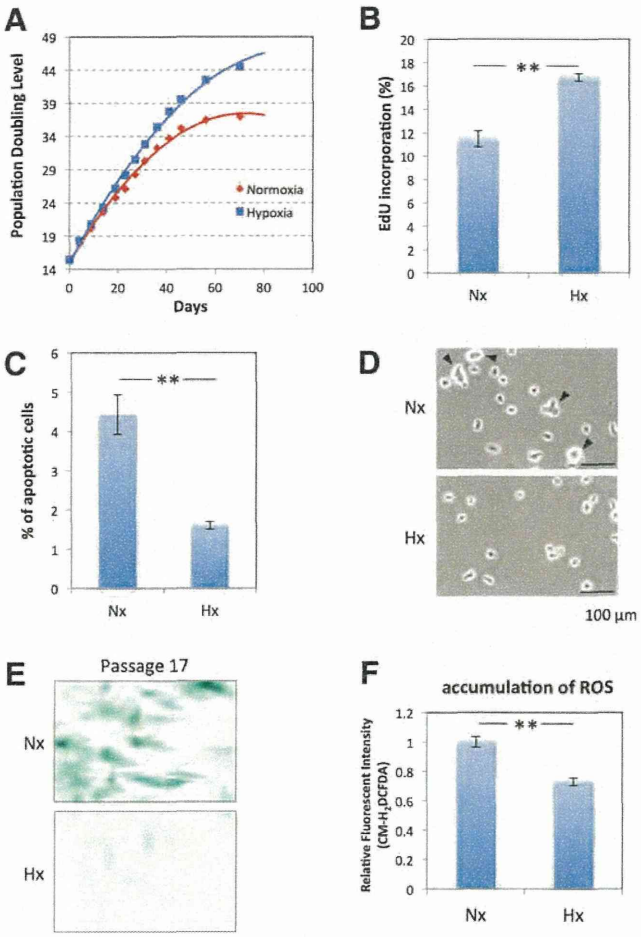

FIG. 1. Hypoxia increases proliferation capacity and decreases senescence in tissue-derived multilineage progenitor cells (hADMPCs). **(A)** Growth profiles of hADMPCs under normoxic (*red square*) and hypoxic (*blue square*) conditions. The population doubling level (PDL) was determined to be 0 when cells were isolated from human adipose tissue. Cells were maintained until they reached PDL13–15 (passage 3) and then split into four aliquots of equal cell densities. PDL was calculated based on the total cell number at each passage. **(B)** Detection of normoxic (Nx) and hypoxic (Hx) cells by flow cytometry after incorporation of EdU. **(C)** Percentages of apoptotic cells with sub-G1 DNA under Nx and Hx conditions. The results are presented as the mean of three independent experiments. **(D)** hADMPCs cultured under Nx and Hx conditions were harvested by trypsin-EDTA and then imaged using a phase-contrast microscope. *Arrowheads* indicate cells with a larger and more irregular shape. **(E)** Cells expanded under Nx and Hx conditions were stained with SA-β-gal. **(F)** Cellular reactive oxygen species detection by the oxidative stress indicator CM-H_2DCFDA in hADMPCs under Nx or Hx. Data are presented as the mean fluorescence intensity of three independent experiments. Error bars indicate SD. $^{**}P < 0.01$ indicates significant difference (independent *t*-test) between Nx and Hx. Scale bars; 100 μm. Color images available online at www.liebertpub.com/scd

genomic DNA of the hADMPCs, and the amount of incorporated EdU was quantified by flow cytometry. As shown in Fig.1B, the EdU incorporation rate was significantly higher in Hx-cultured hADMPCs than in Nx-cultured hADMPCs, suggesting that cell growth was increased in the Hx culture condition. In addition, measurement of DNA content in hADMPCs revealed a slight but significant decrease of sub-G1 peaks, which indicates the existence of apoptotic cells with degraded DNA, when the cells were cultured in the Hx condition (Fig. 1C). These data suggest that the Hx culture condition increases the proliferation capacity of hADMPCs by promoting their cell growth and survival rates. We also found that Nx-cultured hADMPCs were larger with a more irregular shape (Fig. 1D), which suggests that the Hx culture condition prevented hADMPCs from entering senescence [35]. To further investigate this phenomenon, cellular senescence was measured by staining for SA-β-Gal, which revealed that SA-β-Gal activity was increased in Nx-cultured hADMPCs at passage 17 (Fig. 1E). Since it has been hypothesized that senescence results from oxidative stress [20], accumulation of ROS in hADMPCs was detected using the nonfluorescent probe, CM-H_2DCFDA. Flow cytometry analysis revealed that ROS were generated at higher levels in hADMPCs when cultured in the Nx condition (Fig. 1F), suggesting that reduced production of ROS in the Hx condition may prevent the cells from entering replicative senescence.

Hypoxic culture maintains some MSC properties and increases differentiation

We then examined the cell properties of hADMPCs under Nx and Hx conditions. Initially, cell surface antigens expressed on hADMPCs were analyzed by flow cytometry. No significant difference in expression profile between hADMPCs cultured in Nx and Hx was observed; the cells were consistently positive for CD10, CD13, CD29, CD44, CD49a, CD49b, CD49c, CD49d, CD49e, CD51/61, CD54, CD59, CD73, CD90, CD98, CD105, CD166, and HLA-A, B, C, but negative for CD34, CD45, CD117, and CD133 (Fig. 2 and data not shown). These data were consistent with previous reports describing the expression profiles of cell surface markers of hMSCs [36,37]. To further examine the stem cell properties of hADMPCs, their potential for differentiation into adipocyte, osteocyte, and chondrocyte lineages was analyzed at passage 8. Hx-cultured hADMPCs presented enhanced differentiation into various lineages (Fig. 3A, B), indicating that the Hx culture condition improved the stem cell properties of hADMPCs.

Hypoxic culture condition activates Notch signaling

To reveal the molecular mechanism by which the Hx culture condition increased the proliferative capacity and maintained the stem cell properties of hADMPCs, we next examined Notch signaling, which is required for maintaining stem-cell features of various types of stem cells [30,31]. As expected, levels of cleaved NOTCH1, an activated form of NOTCH1, were significantly increased (greater than twofold) in the Hx culture condition (Fig. 4A). Q-PCR analysis revealed that HES1, a downstream target of Notch signaling, was upregulated in Hx-cultured hADMPCs, which also indicated that Notch signaling was activated in

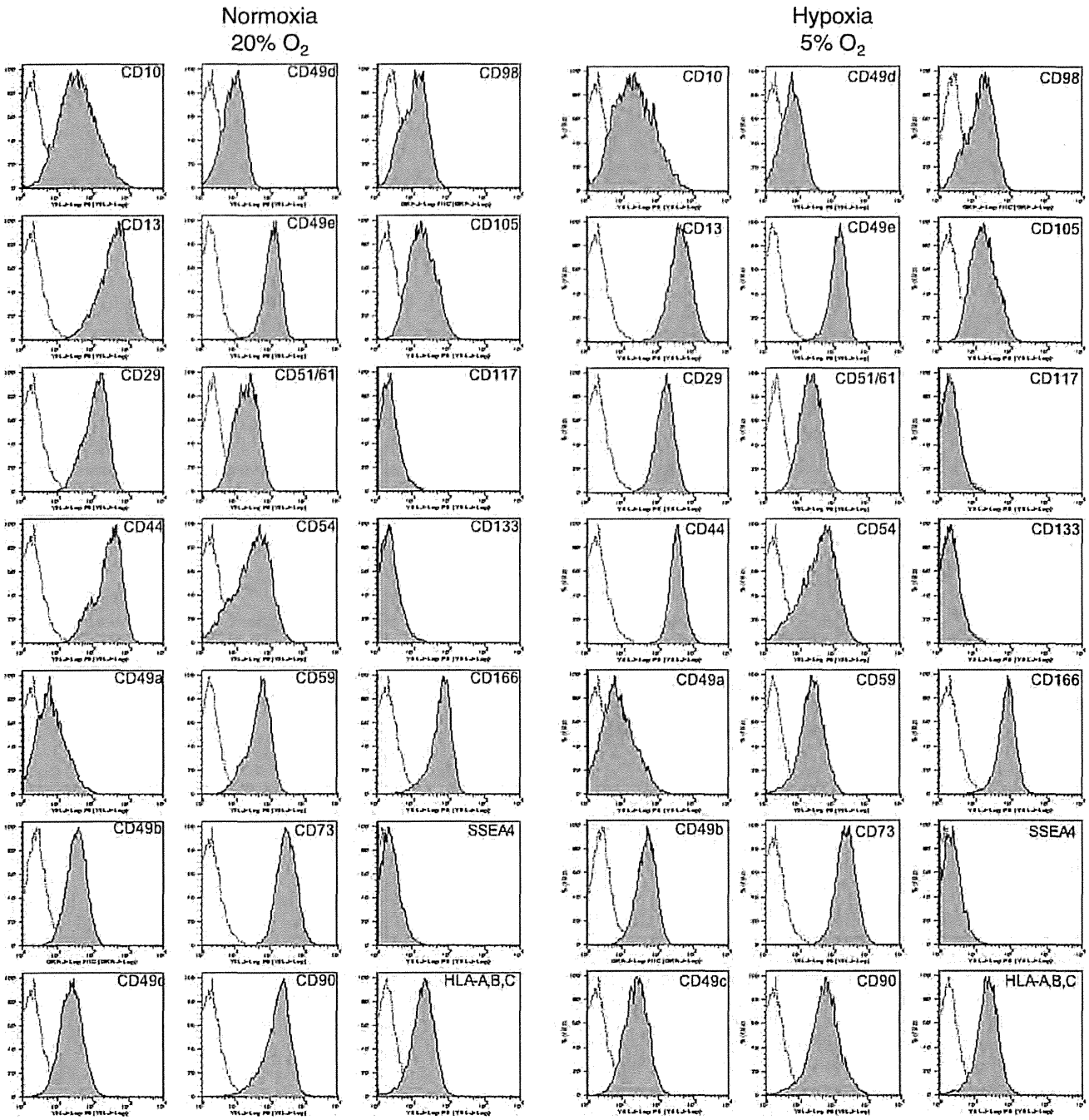

FIG. 2. Hypoxic culture maintains mesenchymal stem cell properties. hADMPCs cultured under normoxia (20% O_2) or hypoxia (5% O_2) were labeled with antibodies against the indicated antigens and analyzed by flow cytometry. Representative histograms are shown. The respective isotype control is shown as a *gray line*.

the Hx culture condition (Fig. 4B). Administration of the γ-secretase inhibitor DAPT at 1 μM, which was sufficient to inhibit the proteolytic cleavage of NOTCH1 (Fig. 4A), decreased the Hx-induced expression of HES1 at both mRNA and protein levels (Fig. 4B, C). These data indicate that Hx increased the expression of HES1 through activation of Notch signaling. It has been reported that Notch signaling and hypoxia-inducible factor (HIF) undergo crosstalk in hypoxic cells [38–41]. Therefore, HIF-1α and HIF-2α protein levels in hADMPCs were analyzed by western blotting. HIF-1α was stabilized when a chemical hypoxia-mimicking agent, cobalt chloride, was applied in the culture; whereas no obvious increase of HIF-1α was observed in the Hx culture condition (Fig. 4D). However, we did not detect any HIF-2α expression even in the presence of cobalt chloride (Fig. 4E). Q-PCR analysis revealed that *HIF2A* mRNA was not expressed in these cells (data not shown). From these results, we concluded that neither HIF-1α nor HIF-2α was involved in the Hx-induced increase in the proliferative capacity and stem cell properties of hADMPCs.

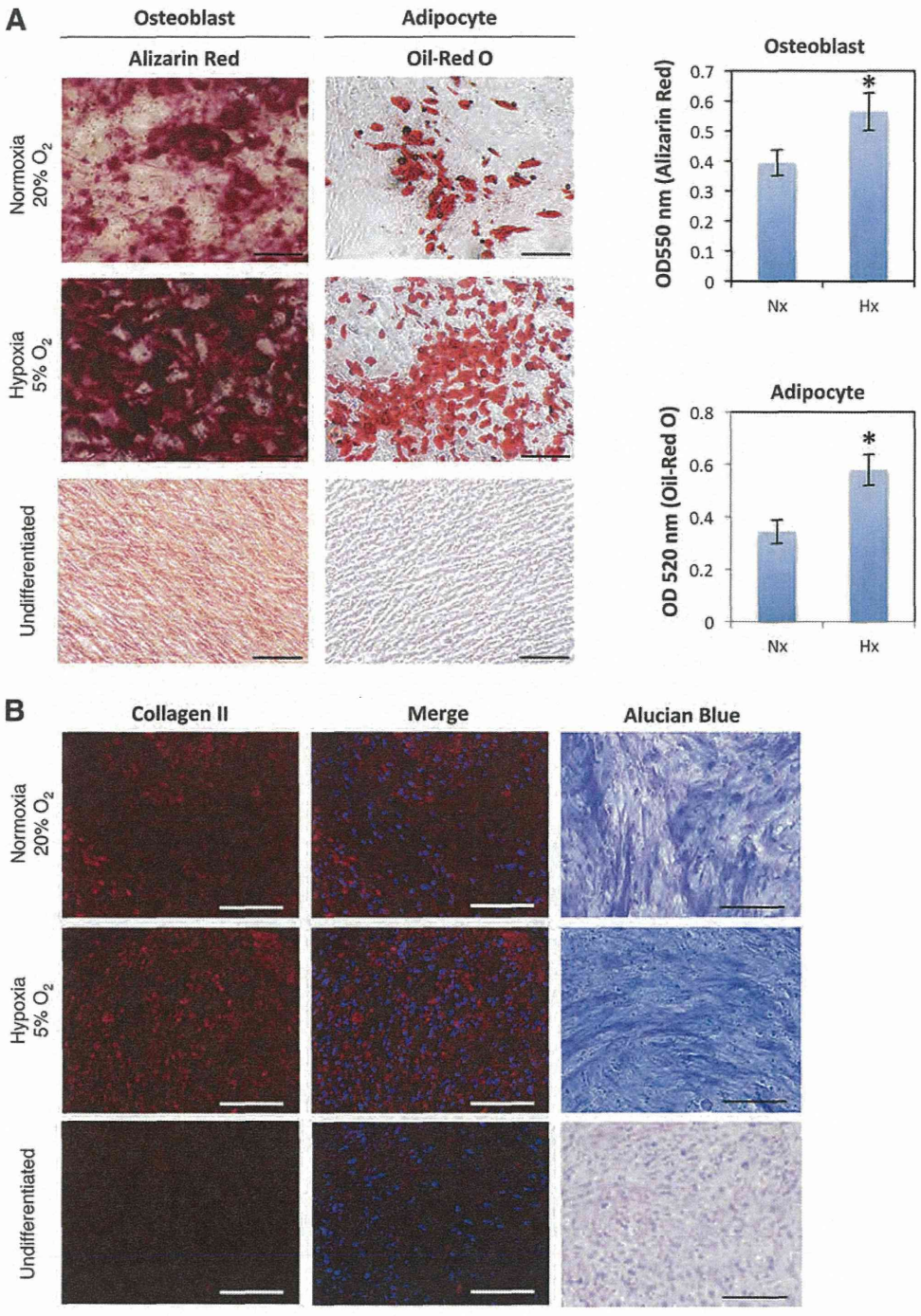

FIG. 3. Hypoxic culture enhances stem cell properties. hADMPCs were expanded under normoxic and hypoxic conditions. **(A)** Normoxic (20% O_2) and hypoxic (5% O_2) cells at passage 8 were induced for 3 weeks to differentiate into osteoblasts and adipocytes and stained with Alizarin Red and Oil-Red O, respectively. The stained dye was extracted, and OD values were measured and plotted as the means of three independent experiments ± SD. $*P < 0.05$. Scale bars, 200 μm. **(B)** Normoxic (20% O_2) and hypoxic (5% O_2) cells at passage 8 were induced for 3 weeks to differentiate to chondrocytes, and immunofluorescent analysis of collagen II (*red*) and Alucian Blue staining were performed. The *blue* signals indicate nuclear staining. Scale bars, 100 μm. Non-induced control cultures in growth medium without adipogenic, osteogenic or chondrogenic differentiation stimuli are shown (Undifferentiated). Color images available online at www.liebertpub.com/scd

To identify the signaling responsible for the observed effect, we next examined the Akt, NF-κB, and p53 signaling pathways. It has been reported that hypoxic conditions induce the activation of Akt and NF-κB signaling [42,43]. In addition, hypoxic conditions have been shown to inhibit p53 activity [44], and crosstalk between these pathways and Notch signaling has also been demonstrated [41,45–47]. As shown in Fig. 4F, the Hx condition increased Akt phosphorylation, which was not decreased by DAPT treatment. These data demonstrate that 5% oxygen activated Akt signaling but not via Notch signaling. Similarly, the hypoxic condition induced nuclear accumulation of p65, which was inhibited by DAPT treatment (Fig. 4G). These data suggest that NF-κB signaling is regulated by Notch signaling in hADMPCs. Furthermore, p53 was not activated under the 5% oxygen condition as assessed by detection of phospho-p53 and a p53 reporter assay. However, DAPT treatment significantly increased p53 activity (Fig. 4H, I).

Notch signaling is indispensable for acquisition of the advantageous properties of hADMPCs

We next examined the roles of Notch signaling in the proliferative capacity and stem cell properties of hADMPCs